Fall 1-31-2014

Mathematically modeling the mechanical constants of thoracolumbar fascia under compression, in vivo

Vrajeshri Patel
New Jersey Institute of Technology

Copyright Warning & Restrictions

The copyright law of the United States (Title 17, United States Code) governs the making of photocopies or other reproductions of copyrighted material.

Under certain conditions specified in the law, libraries and archives are authorized to furnish a photocopy or other reproduction. One of these specified conditions is that the photocopy or reproduction is not to be "used for any purpose other than private study, scholarship, or research." If a, user makes a request for, or later uses, a photocopy or reproduction for purposes in excess of "fair use" that user may be liable for copyright infringement,

This institution reserves the right to refuse to accept a copying order if, in its judgment, fulfillment of the order would involve violation of copyright law.

Please Note: The author retains the copyright while the New Jersey Institute of Technology reserves the right to distribute this thesis or dissertation

Printing note: If you do not wish to print this page, then select "Pages from: first page # to: last page #" on the print dialog screen

ABSTRACT

MATHEMATICALLY MODELING THE MECHANICAL CONSTANTS OF THORACOLUMBAR FASCIA UNDER COMPRESSION, IN VIVO

by
Vrajeshri Patel

The thoracolumbar fascia (TLF) is a complex structure made of many interconnecting aponeurosis and muscle fascia. It plays a role in posture, stabilizing the lumbosacral spine, load transfer, and respiration. Its complex structure and connections have mostly been observed through cadaveric studies while its mechanical properties have been addressed in only a few studies. Recently, new advances in ultrasound imaging have made it possible to move towards measuring tissue strain. Since this is an in vivo method, mechanical data of tissues in their natural environment allows a more accurate representation of tissue strain. However, many different methods of analyzing ultrasound data have been proposed.

In this study, the posterior layer of the TLF (pTLF) is studied under compression using ultrasound imaging in order to determine its mechanical properties. Using B mode imaging, deformation is measured in skin, fat, TLF, and the underlying erector spinae muscles using a tracking algorithm developed in Matlab. Data analysis is then used in a nonlinear mathematical model and a finite element model to quantitatively evaluate mechanical constants. Although TLF mechanical constants are not available for comparison, estimates of the modulus of elasticity of skin, superficial fascia, pTLF and the erector spinae muscle group are within an acceptable physiological range.

MATHEMATICALLY MODELING THE MECHANICAL CONSTANTS OF THORACOLUMBAR FASCIA UNDER COMPRESSION, IN VIVO

by
Vrajeshri Patel

A Thesis
Submitted to the Faculty of
New Jersey Institute of Technology
in Partial Fulfillment of the Requirement for the Degree of
Master of Science in Biomedical Engineering

Department of Biomedical Engineering

January 2014

APPROVAL PAGE

MATHEMATICALLY MODELING THE MECHANICAL CONSTANTS OF THORACOLUMBAR FASCIA UNDER COMPRESSION, IN VIVO

Vrajeshri Patel

Dr. Hans R. Chaudhry, Dissertation Advisor — Date
Research Professor, NJIT

Dr. Thomas Findley, Committee Member — Date
Professor, Rutgers New Jersey Medical School

Dr. Max Roman, Committee Member — Date
Assistant Research Professor of Biomedical Engineering, NJIT

Dr. Bharat B. Biswal, Committee Member — Date
Professor of Biomedical Engineering and Chair, NJIT

BIOGRAPHICAL SKETCH

Author: Vrajeshri Patel

Degree: Master of Science

Date: January 2014

Undergraduate and Graduate Education

- Master of Science in Biomedical Engineering
  New Jersey Institute of Technology, Newark, NJ, 2014

- Bachelor of Science in Engineering Science,
  New Jersey Institute of Technology, Newark, NJ, 2012

Major: Biomedical Engineering

I dedicate this thesis to my family who puts up with me through stressful times.

ACKNOWLEDGMENT

I would like to thank my thesis advisor, Dr. Hans Chaudhry, for his patience and guidance through this thesis project. His curiosity for learning new things always motivated me to work harder and never give up. I would also like to thank Dr. Thomas Findley for teaching me how to mold a project into a workable plan and opening the door for collaborative research at the Veterans Affairs Center in East Orange. Many thanks go to Dr. Max Roman for offering his time and expertise in this project. His inputs allowed me to think in new directions. I would also like to thank Dr. Bharat Biswal for being a part of my thesis committee. Last, I want to thank my sister, Dharni Patel, for allowing me to practice ultrasound imaging on her for many long hours.

TABLE OF CONTENTS

TABLE OF CONTENTS
(Continued)

Chapter **Page**

LIST OF TABLES

LIST OF FIGURES

CHAPTER 1

INTRODUCTION

1.1 Background Information

The thoracolumbar fascia (TLF) is a complex structure made of many interconnecting aponeurosis and muscle fascia that plays a role in posture, stabilizing the lumbosacral spine, load transfer, and respiration (Willard et al., 2012). It has been a target for manual therapy for many years but only recently has its relationship with low back pain as well as shoulder and leg pain been studied. Its complex structure and connections have mostly been observed through cadaveric studies while its mechanical properties have been addressed in only a few studies (Langevin et al.,2009 and Langevin et al., 2011).

Recently, new advances in ultrasound imaging have allowed it to move towards measuring tissue strain (Ophir et al.,2002). Since this is an *in vivo* method, mechanical data of tissues in their natural environment allows a more accurate representation of tissue strain. However, many different methods have been proposed to measure this strain. For example, static elastography uses inherent echo reflections to measure the distortion of tissues after applying stress. Other methods include measuring echo intensity, digital image correlation, or direct measurements taken from B mode, M mode, or Doppler mode analysis.

The biomechanical properties of tissues such as tendons, ligaments, and muscles are usually described by their modulus of elasticity, or Young's Modulus, by testing the tissue under tension. However, this only describes a linear stress-strain relationship under lower stresses. Additionally, tissue stiffening at higher stresses and viscoelastic properties cannot be seen in this region. Therefore, a model to describe the non-linear

stress-strain curve across both lower and higher stresses is needed to more adequately characterize a tissue. The mathematical model used here uses mechanical constants, C_1 and C_2, in order to describe the stress-strain curve of skin, fat, deep fascia, and the underlying muscle in the low back. C_1 is analogous to the modulus of elasticity and C_2 is a dimensionless constant. This model can be used on any type of soft tissue under stresses in three dimensions.

1.1.1 Objective

In this study, the posterior layer of the TLF is studied under compression using ultrasound imaging in order determine its mechanical properties. Using B mode imaging, deformation is measured in skin, fat, TLF, and the underlying erector spinae muscles. Analysis is then extended to a mathematical model that describes the deformation of soft tissues that may be seen during manual therapy. This study serves as a basis for which other tissues, especially those in a pathological state or tissues subject to manual therapy, can be studied *in vivo*.

1.1.2 Limitations

Raw radio frequency data from the ultrasound machine used in this study could not be collected. Therefore, B mode images generated from the machine were directly analyzed after image noise reduction. Since a new method of analyzing images is proposed, the data in this thesis is subject to interpretation. Additionally, data from only two subjects is available to create the proposed model. Additional data sets will be needed to verify the results.

1.1.3 Outline

Chapter 2 reviews fascia and describes the thoracolumbar fascia in detail. Ultrasound imaging is also discussed. Chapter 3 describes methods of data acquisition and analysis. This chapter will also further detail how biomechanical properties of soft tissues are measured. Results are presented in Chapter 4 and Chapter 5 concludes the study.

1.2 Fascia

When learning human anatomy, the body is often divided into systems such as the skeletal, muscular, and nervous systems. Medical students learn that a nerve innervates a certain muscle causing the muscle to contract and its skeletal counterpart to move. The problem behind this type of approach is that the complexity behind human movement is lost, and other approaches are often ignored. For example, during a human cadaver dissection, connective tissues overlying muscles are often removed to study how muscles connect and produce coordinated movement. Interestingly, surgeons, physiatrists, physical therapist, osteopaths, and other professionals have called for a closer look at the connective tissues found throughout the body.

Fascia, in a rather general definition, is continuous matrix of connective tissue proper that extends through the entire body. The connective tissue matrix, composed of ground substance and different types of fibers, varies according to the location and function of different fasciae. According to the Federative International Committee on Anatomical Terminology (1998) and other anatomical literature, fascia is composed of irregularly arranged collagen fibers, differentiating it from the regularly arranged bundles of collagen fibers found in tendon and ligaments. It is also then differentiated from

aponeurosis in that aponeurotic tissue is similar to a flattened tendon, or sheet, with regularly arranged collagen fibers. An irregularly arranged collagen matrix allows fascia to sustain stress in multiple directions. However, a deeper level of research shows that fascia in many areas may be more organized (Benetazzo et al., 2011) while other research shows that limb and trunk fascia differ in the number of layers (C. Stecco et al., 2006) and composition (Gerlarch, U. & Lierse, W., 1990). This thesis uses the model developed in Benetazzo (2011) which is consistent with other reviews (Willard et al., 2012 and Benamin, 2009). In this model, the thoracolumbar fascia is made of alternating loose connective tissues and dense regular connective tissues.

Since this thesis studies the thoracolumbar fascia under compressive forces, it is important to consider the layers that lie above and below the fascia during compression. Fascia can be generally classified into four different types: pannicular/superficial, deep/investing, meningeal (surrounds central nervous system), and visceral (surrounds body cavities) (Willard et al., 2012). A study done by (Lancerotto et al., 2011) shows that the subcutaneous tissue throughout the body can be divided into a superficial adipose layer and a deep adipose layer with a membranous layer dividing the two (Figure 1.1).

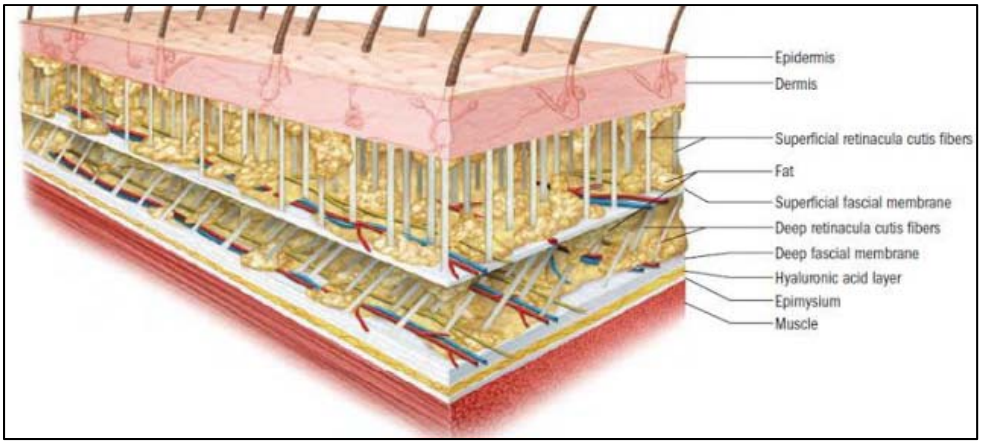

Figure 1.1 shows the three layers of the superficial fascia. Notice vertical retinacula in the superficial adipose layer and obliquely-horizontally orientated retinacula in the deep adipose layer.
Source: Joe Muscolino. Fascial Structure. Massage Therapy Journal, Spring 2012.

The superficial fascia can be considered to include all three layers or just the membranous layer. The superficial adipose layer is made of large fat lobes encased between fibrous septa, or the retinacula cutis superficialis, which is orientated perpendicular to the surface and connects the dermis with the layers below. On the other hand, the fibrous septa, or the retinacula cutis profunda, in the deep adipose layer is orientated obliquely-horizontally and connects to the deep fascia. The membranous layer's thickness and composition can vary greatly through the body and in some areas cannot be identified through dissection. In the area investigated here, ultrasound imaging was able to detect this layer only in subjects with a larger subcutaneous fat layers or once compression was applied.

The membranous layer of superficial fascia is a fibro-elastic tissue with abundant well organized elastin fibers. Histologically, it can be formed from only one to several interconnecting sublayers depending on the location in the body. It contains nerves and vessels, but the orientation and structure of branching still requires further study.

Together with the superficial adipose layer and the deep adipose layer, a gliding system is created in the subcutaneous tissue so that the overlying skin is free to move independently. It also absorbs the mechanical stimulations applied to the skin or generated by muscular contractions (L. Stecco et al., 2009).

Below the superficial fascia is the deep, or investing, fascia found around the musculoskeletal system. The term "investing" is used because it blends into the periosteum of bone, epimysium of skeletal muscles, and peritoneum of tendons and ligaments. However, it also extends from a muscle to its respective aponeuroses. This type of fascia is thicker and denser than other types of fascia and is found surrounding all bones, cartilages, muscles, tendons, ligaments, and aponeuroses.

Anatomical and histological studies have shed light on not only the continuity of the deep fascia throughout the body, but also offer a correlation between its structure and function. C. Stecco (2006) characterizes the brachial and antibrachial fascias as multiple layers of parallel, undulating collagen fiber bundles, with a specific orientation. Each layer is separated by a thin layer of adipocytes. This adipocyte layer is thought to allow for gliding between adjacent layers. However, in some areas, the fascial layer adjacent to the epimysium of muscle is directly connected via collagen bundles. Fibroblasts are arranged between and parallel to collagen fiber bundles. Short, branched elastin fibers were seen between collagen bundles forming an irregular mesh. A similar composition was found in the crural fascia, which surrounds the muscles of the thigh, with a few distinctions. C. Stecco (2009) distinguished three layers in the crural fascia. Each layer was composed of parallel, undulating collagen bundles in a certain orientation and separated from its adjacent layer by loose connective tissue. Benetazzo (2011) found an

angle of 78º + - 4.3 degrees between adjacent layers in the posterior layer of thoracolumbar fascia. Some points in the tissue were also found to adhere to the underlying muscle. Elastin fibers were found in loose connective tissue layers, but scarcely so in the fibrous layers.

The multilayered structural arrangement found in both the upper limb and crural fascia shows that deep fascia is able to resist loads in multiple directions in the plane of fascia because of different collagen orientations. Elastin fibers and undulating collagen fibers may allow fascia to stretch and relax when traction is applied and removed. Loose connective tissue layers between fibrous layers ease sliding between layers. It may also serve a role in allowing adaptability during contraction of underlying muscles. Additionally, upward pressure loads resulting from muscle contraction may equilibrate by causing tensile stresses in the plane of fascia. The force transduction between muscle and its overlying fascia is of great interest. For example, in compartment syndrome fascia may not be able to expand to accommodate tension caused by the underlying muscle, causing an increase in pressure of the compartment below it and affectively disrupting blood flow and nerve pathways. In both types of fasciae, some areas showed a direct connection to the underlying muscle. Although it is not known whether this phenomenon is physiological or pathological, a reduction in sliding would be seen at this point.

1.3 Functions of Fascia

Fascia has many functions relating to musculoskeletal dynamics. These range from its role as an ectoskeleton by supplying additional muscle attachments, the importance of creating osteofascial compartments for muscles, encouraging venous return in the lower limbs, dissipating stress concentration at entheses and acting as a protective sheet for underlying structures. In order to understand how fascia accomplishes these various functions, a better understanding of its *in vivo* biomechanical properties is needed.

1.3.1 Role in Muscular Contraction

Muscles, joints, bones, and interweaving fasciae work in unison to create simple to complex movements. In many areas, several muscles of varying architecture work in synergy over the same joint. These muscle groups are contained and organized in fascial compartments (Purslow, 2002). Each segment of a limb has its own compartment separating functional groups of muscles based on embryological origins, blood and nerve supplies. Organized collagen fibers in fascia layers surrounding muscle groups in the body suggest that they may play a more important mechanical role than previously thought (Aspden, 1990).

Purslow (2002) offers one explanation of how synergist muscles packed in compartments created by fascia increases efficiency of muscle contraction. Contraction of one muscle within the compartment raises the pressure by 15 mmHg in normal contraction and 80 mmHg in tetanic contractions. This raises the contractile efficiency of all muscles in the compartment. The surrounding fascial sheaths do not allow for increased volume of the compartment as muscle tissue volume increase and decrease during contractions; this results in increased compartment pressure (Westneat et al.,

1998). Constraining lateral muscular expansion by surrounding it with a strong fascia may therefore increase the strength and stiffness of the muscle by about 5 to 10% at low pressures for any given length of contraction (Aspden, 1990). Conversely, cutting the fascia releases 50% of this normal pressure generation and decreases contractile force by 16% (Garfin et al, 1981). Cutting fascia requires surgeons to be aware of the nerves and blood vessels that travel through fascia; less consideration is given to alterations of mechanical strength post-operatively. In the search for optimal surgical technique, this should also be considered.

During knee extension, the thousands of available knee extensor fibers from various muscles do not all activate simultaneously. The degree of extension may be controlled by a feedback/feedforward mechanism in the myofascial unit (comprised of muscle fibers from different muscles, interweaving fasciae, and the articulation they act upon) (L. Stecco et al., 2004). Fascia is subjected to different tensions according to the degree of joint movement and therefore, is able to vary recruitment of relative muscle fibers. On the coordinating level, Stecco describes how many muscles are able to work in synchrony in order to move a joint in one direction. Fascial "bridges" unite the many muscles that act on one joint by focusing the contractile force towards a single point of reference, or center of coordination.

1.3.2 Force Transmission and Ectoskeleton

Smeulder (2005) showed that up to 37% of maximal muscular force can be transmitted to inter and extramuscular connective tissues rather than on muscle's tendon directly . The different fasciae found in a myofascial unit may serve a role in force transmission. As muscles contract, generated forces may transfer to extramuscular tissues such as

intermuscular septa, fascial sheaths, periosteum, and interosseous membranes (Huijing et al., 2009). Muscle forces can then transmit to joint capsules, ligaments and other muscles within the compartment.

In areas such as the back and lower limb, fascia is thicker because of the many muscular attachments. As described above, fascia connects not only muscles, but has connections to bones, ligaments, and tendons. Many authors in the field of fascia research therefore refer to fascia as a soft tissue skeleton, or ectoskeleton, first coined by anatomist Frederic Wood Jones in 1944. The musculoskeletal system is responsible for the human body's ability to maintain an upright posture as well as agile movement. This can be especially seen in the lower leg where the gluteus maximus and tensor fascia latae attach predominantly to the deep fascia rather than bone. C. Stecco (2007) shows that fascia is stretched at to a basal tension by its muscular insertions. When the muscles contract, the attached fascia further tenses; this may influence other parts of the body through its continuities (L. Stecco et al., 2004).

1.4 Thoracolumbar Fascia

1.4.1 Structure

The TLF is modeled as three layered versus two by many anatomists (Bogduk and Macintosh, 1984, Standring, 2008). As seen in Figure 1.2, the anterior layer is found anterior to the quadratus lumborum and laterally joins the middle layer of the TLF which passes between the paraspinal muscles and the quadratus lumborum muscle. The posterior layer of the TLF, or pTLF, which is studied in this thesis, surrounds the paraspinal muscles (ileocostalis, longissimus, and multifidus). The ileocostalis and

longissimus blend in the lumbar region to form the erector spinae muscle group. All three layers join laterally at the lateral ralphe.

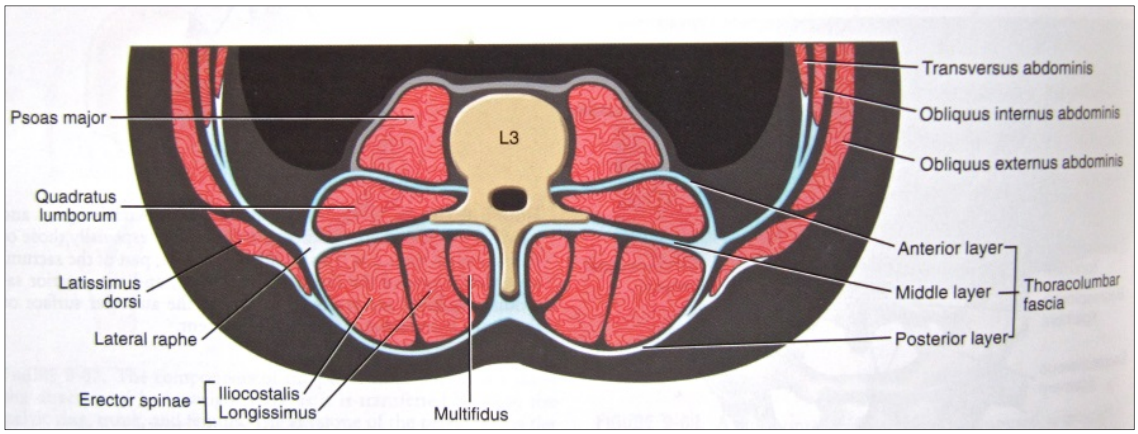

Figure 1.2 Diagram of the muscle of the back and the different layers of thoracolumbar fascia surrounding them.
Source: Neumann, Donald A. *Kinesiology of the musculoskeletal system*. Mosby/Elsevier, 2002.

The subdivision of the pTLF are still under investigation in cadaver studies. The names given to each layer vary according to the author and the region of TLF studied. In this study, the region in consideration is located at L2, L3 level and two centimeters lateral to the spinous process. Here, the pTLF will be considered as divided into a superficial layer and a deep layer (Willard et al., 2012) that is separated by a layer of loose connective tissue. The superficial layer is further divided into two layers. See Figure 1.3.

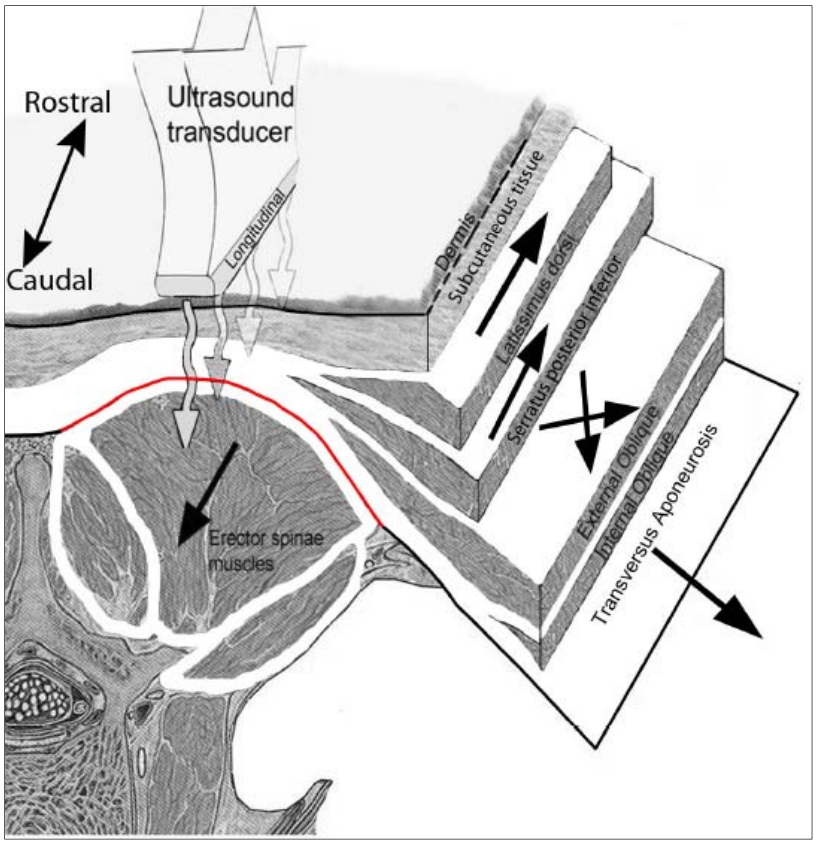

Figure 1.3 The layers that make up the posterior layer of the thoracolumbar fascia can be seen here. The superficial layer is made of the lattisimus dorsi and serratus posterior inferior muscle epimysiums. The deep layer is made from the paraspinal retinacular sheath that covers the erector spinae muscles. The red line shown in the diagram represents the loose connective tissue layer that separates both layers. This diagram also shows where the ultrasound probe is placed.
Source: Langevin, Helene M., et al. "Reduced thoracolumbar fascia shear strain in human chronic low back pain." *BMC musculoskeletal disorders* 12.1 (2011): 203.

The first layer is made of the thin epimysium of the latissimus dorsi and the latissimus dorsi epimysium. Although the serratus posterior inferior muscle ends at the twelfth rib, its aponeuroses continues down into the upper lumbar level to make the second layer of the superficial lamina (Willard et al., 2012, Benetazzo, 2011). According to a histological analysis by Benetazzo (2011) the fiber angle between these two layers is 78 degrees. The deep layer of the pTLF is actually the paraspinal retinacular sheath that covers the paraspinal muscles. The orientation of fibers has been debated by many

studies of this area. However, many agree that the fibers generally run 20-30 degrees below the horizontal. (Vleeming et al. 1995, Bogduk et al.,1992) Laterally, the seratus posterior inferior aponeurosis fibers blend with the latissimus dorsi fibers above and the deep lamina below. In the region being studied however, the superficial and deep lamina are still distinct.

Considering the entire back, the superficial layer of the pTLF extends superiorly to the fasia nuchae according to Vleeming (2007). Bogduk (1992) found that the superficial layer passes under the trapezius and rhomboids in the cervical region while Barker (2004) found it to fuse with these muscles. The inferior border, according to Bogduk (1992) attaches to the posterior superior iliac spine as it fuses with the origin of the gluteus maximus. Willard (2012) proposes that the deep lamina extends from the sacrum to the splenius capitis and eventually fuses to the cranial base at the nuchal line with the cervical fascia. Laterally and inferiorly, the deep lamina fuses over the iliac crest with the aponeurosis of the gluteus medius. More medially and inferior, the deep and superficial laminae fuse together at the level of PSIS. Below PSIS, this combined aponeurotic structure extends laterally to create an intermuscular septum to which the gluteus maximus attaches in a bipennate arrangement (Willard, 2012).

1.4.2 Innervation of the Posterior Layer of the TLF

The low back is a common site for injury and pain. However, the cause of low back pain and whether it leads to physiological changes or results from physiological changes is largely unknown. While some nerves and blood vessels may only pass through fascia, many studies have found abundant innervation of the superficial and deep fasciae. A

closer look at the innervation of the TLF contributes to a better understanding of low back pain and the functions of the TLF.

L. Stecco (2009) proposes that mechanoreceptors, like Pacini corpuscles, are found in the three layers of the superficial fascia as described previously. The gliding system of the superficial fascia allows autonomy between skin and deep fascia. However, if this gliding system is disrupted, by scar formation for example, the skin, superficial fascia, and deep fascia begin to adhere to each other and the extracellular matrix becomes more viscous. Any external stimuli is then transmitted to the deep fascia and underlying muscles. Vice versa, any muscular contractions can be transmitted to mechanoreceptors in skin. Additionally, if this superficial fascia stiffens, the pathway of nerves and vessels becomes constrained. This can cause an abnormal pull on nerves resulting in hyper-activation and sensitivity.

More histological studies are available on the deep fascia. Widespread termination of small sensory neurons in rat (Corey et al., 2011) and human lumbar fascia (Tesarz et al., 2011) supports the notion that deep fascia is highly innervated. Abundant sympathetic fibers found accompanying blood vessels have been observed (Tesarz 2011), suggesting a vasomotor function of deep fascia. Tesarz (2011) also found that these sympathetic nerves branch into the collagen fibers of pTLF in rats. This suggests that a relationship between the sympathetic nervous system and pathophysiology of facial disorders. Furthermore, stimulation of these intrafascial sympathetic nerve fibers may trigger modification in terms of autononomic nervous system tone, circulation, and matrix hydration (Schleip 2011).

Pacini corpuscles that sense touch and vibration and Ruffini corpuscles that sense stretch have been found in the supraspinous, interspinous, and iliolumbar ligaments of the vertebrae. Golgi tendons that sense muscle tension have been found in the iliolumbar ligaments. The pTLF's attachment to these layers as it connects medially to the spinous process and vertebrae support its role in proprioception, or the sense of mechanical forces within the body. O'sullivan (2003) found a connection between low back pain and reduced lumbar proprioception while Lambertz (2006) found that inhibition of proprioceptive signaling augments pain sensitivity in rats. Some manual therapy and exercise programs may cause increased proprioception in patients with low back pain.

The TLFs nociceptive function has also been studied by a few authors. Dittrich (1963) found signs of injury and inflammation in TLF taken from patients with low back pain. However, there is no healthy control to compare these samples with, so physical changes could also be from aging. Tesarz (2011) found nerve endings in the superficial layer and loose connective tissue layers of the pTLF, but not the deep layer. The question now becomes whether stimulating nociceptive receptors could cause low back pain. Taguchi (2008) showed that pinching the TLF and applying a hypertonic saline in rats elicited a response in many neurons in the dorsal horn of the spinal cord, suggesting a nociceptive response.

1.4.3 Biomechanics of the TLF

As previously stated, the TLF has an anterior, middle, and posterior layer. The pTLF is made of multiple layers of collagen fibers. An individual collagen molecule is made of alpha protein chains. Collagen molecules bundled together are called collagen fibrils, which then form a larger unit called the collagen fiber. Collagen fibers in the TLF and

other fascia have been characterized as undulating, or wavy. When a small amount of tension is placed on collagen fibers, they have large strain because this wavy pattern is straightened. They then exhibit elastic behavior similar to Hooke's law until a plastic region is reached and ultimately, a failure point. Collagen fibers are generally subject to tensile forces. However, it has been shown that they also contribute to compressive stiffness in intervertebral disks (Romgens et al., 2013).

Myofibroblasts are connective tissue cells with an increased contractile force and are responsible for wound closure. They have also been found in the collagen layers of TLF. They may increase in number as a result of mechanical strain and changes in the biochemistry of its surroundings (Tomasek et al., 2002). Sympathetic activity increases cytokine tumor growth factor which stimulates myofibroblast activity. The origin of myofibroblast proliferation can be mechanical, chemical, or neural, and may lead to an increase in stiffness and decrease in elasticity.

Many more studies have looked at the stiffening of fascia from a biomechanical approach. Fascia is a viscoelastic material, so it exhibits time dependent strain (see Figure 1.4). In the small strain region, collagen fibers are still aligned in waves and most stretching is due to elastin fibers. As strain increases, the collagen fibers begin to align in the direction of the strain and eventually are straightened (phase III). This is where most resistance to stress is found.

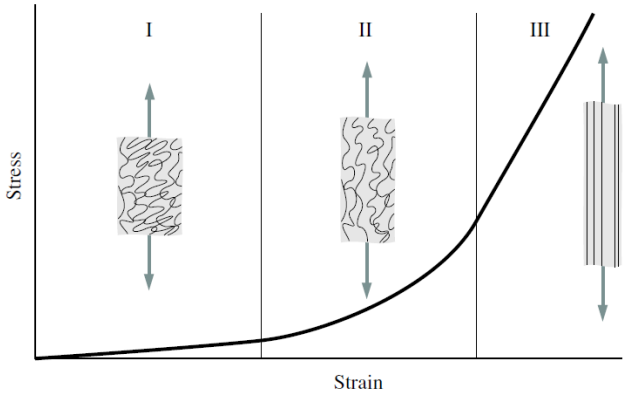

Figure 1.4 Phases of stress-strain curve of a viscoelastic material.

Yahia (1993) found that successive stretches of fascia caused stiffening of fascia; after a one hour rest period, strains returned to baseline. A more recent study (Schleip 2012) found evidence of strain hardening after a stretch and rest paradigm. They also found an increase in matrix hydration after the rest time. As the different layers of the pTLF must also glide along each other, shear strain is present. Langevin (2011) found decreased shear strain in chronic low back pain subjects using ultrasound.

The TLF is able to increase by 30% in length when the spine is fully flexed by decreasing in width; the resulting strain energy may allow reduced muscle work as the spine extends to resting position (Adams et al., 2007). Adams (2007) also found that the TLF is strongest when the back is in a relatively straight posture flattening the lumbar lordosis. At this lumbar level there is an average distance of 62 mm between the center of the intervertebral disk and the TLF. If the center of motion is at the vertebral body, then this distance allows for a significant extensor moment without creating high compressive forces on the vertebral column. According to Gatton (2010), the TLF applies small flexion moments at L2/L3 and L3/L4 and larger extension moments at L4/L5 and L5/S1. Their 3D mathematical model predicts this extension moment in the

upright position to have a magnitude of 7-11 Nm. These studies have considered the biomechanics of the TLF relative to the spine. However, because TLF is essentially made from its surrounding muscles and tissues, it is important to consider how the abdominal, paraspinal, and extremity muscles affect the TLF. An increase in intra-abdominal pressure was mimicked by Tesh (1987) using balloons in cadavers. They found resistance to lateral flexion of the spine and concluded that the middle layer of the TLF contributes as much as 40% of restriction in total flexion. The transverse abdominis aponeuroses connects to the TLF laterally and causes tension in the middle layer of the TLF and increased resistance to flexion at L3/L4. The tension in the TLF affects the erector spinae muscles in the fascial sheath by restricting lumbar flexion. Although these studies need to be verified *in vivo*, the role of the transverse abdominus muscle in lumbosacral spine support via the TLF is evident.

The paraspinal muscles are subject to uniaxial tension which causes strain in the longitudinal and transverse directions. The TLF surrounding these muscles constrains its expansion during contraction and thereby increases the strength and stiffness of the muscles. Because of fascia's viscoelastic effect, rapid contractions of the paraspinal muscles would also increase fascia's stiffening role.

The pTLF especially plays a role in transferring forces between the spine, pelvis and legs because of muscle and aponeuroses insertions to it. The gluteus maximus and latissimus dorsi can transmit forces contralaterally via the pTLF. Contraction of the erector spinae muscles and multifidus is expected to increase tension in the deep lamina of the pTLF as well as cause "inflation" (Gracovetsky et al., 1977). Vleeming (2007)

argues that the pTLF should then be strengthened by exercising the gluteus maximus, latissimus dorsi, erector spinae, and multifidus muscles.

1.5 Ultrasound Imaging

Ultrasound imaging, UI, for medical purposes began in the mid -1940s by Dr. Karl Theodore Dussik of Austria who made his first ultrasound prototype to image the brain. Since then, ultrasound imaging has spread to all parts of the body and many different types of tissues. It serves in the study of anatomy, but is increasingly being used as a diagnostic tool. Recently, ultrasound research has moved towards a new type of imaging technique called elastography which was originally used in the detection of cancerous tumors. A brief overview of ultrasound imaging and its uses is presented here.

"Ultrasound" refers to sound waves above the audible range of human hearing, which is 20 kHz. UI uses typically uses sound waves with a frequency of 2-18 MHz. A transducer is the main component of an Ultrasound machine because it creates and detects sound waves and echoes, respectively. Quartz crystals found in the transducer can rapidly change shapes when an electric current is applied (piezoelectric effect, or pressure electricity). The vibrations resulting from these shape changes cause sound waves that travel outward. Because sound waves do not travel well through air, a gel is placed between the transducer and skin to promote sound waves to transmit through them to the underlying tissues. Transducers come in different shapes, sizes, and frequency ranges. The shape and size determine the field of view. The frequency will determine the depth and resolution of the image. Higher frequencies have less penetration, but

better resolution. Lower frequencies allow detection of deeper tissues at the cost of resolution.

Sound is reflected anywhere there are density changes in the body; some waves will be reflected by each layer while others will continue down to deeper layers until they are reflected by another boundary. The return of the sound wave, or echo, vibrates the crystals again, which emits electric currents that are then digitized by the CPU of the machine. Using the average speed of sound in tissue (1,540m/s), the time of each echo's return, and the intensity of the echo, an image based on calculated distances and intensities is formed. However, the sound of speed through soft tissues varies throughout the body. In fat, it is 1,440 m/s; in muscle it is 1,570 m/s. This assumption causes the beam to de-focus reducing resolution. Research into algorithms that apply a measured speed of light through specific tissues and then use raw ultrasound data to re-create images has allowed for a more refined approach to ultrasound research . In this study, raw data was not able to be collected from the Ultrasound machine available. Other assumptions are that sound travels in a straight line from the direction transmitted and that sound is attenuated equally by different tissues. The average attenuation of .5dB/cm/MHz is used by ultrasound machines. Muscle has an attenuation of 1 dB/cm/Mhz.

Several modes of UI are available on a standard machine. The first UI machines used A mode (amplitude mode), where a single crystal was used to generate the pulses and record echoes. The resulting image is a plot of the amplitude of echoes along a single line as a function of depth. B mode images are more commonly used. The machine used in this thesis has a transducer with multiple crystals in a linear array that

alternate in sending out waves. This allows multiple scan lines to be obtained resulting in a 2D B mode image. Shades of gray represent different echo amplitudes. M mode, or motion mode, combines A mode and B mode to display motion along the y axis. Doppler mode relies on the "Doppler shift" caused by moving tissues. The Doppler shift frequency is the difference between transmitted and received waves. The velocity of the tissue can then be calculated based on this Doppler shift frequency, speed of sound, angle of beam, and transmitted frequency. Elastography, the most recent advance in UI, has been recently used to measure tissue stiffness and elasticity. Its use was first presented in the 1990's, and since has been applied to many parts of the body. In static elastography, a small compression is applied by the user and the displacement of tissue at each depth or distance from the transducer is measured using a cross-correlation function. The rate of change in the amount of tissue displacement is called tissue strain. Tissue strain in soft materials will be large while tissue strain in stiffer tissues will have lower tissue strain values. However, mechanical constants like Young's modulus are still not able to be calculated because applied pressures and tissue boundaries are unknown. However, in terms of detecting a stiff tumor in the middle of healthy tissue, this type of UI is of great value.

Because UI is an in-vivo tool, it allows more reliable measurements compared to cadaver or in-vitro methods. Looking at a B mode image, we are able to see movement of a muscle and tendon during a certain motion. However, quantifying that movement can be difficult because of the high signal to noise ratio of ultrasound b mode images. Using different methods of analysis, this limitation can be overcome. Okotie (2012) used digital image correlation to measure strain in the Achilles tendon of rats. Another

study uses B mode ultrasound image tracking to measure contractile length of the gastrocnemius and soleus muscled during applied ankle torque (Loram et al., 2006). Increased thickness and echogenicity of the pTLF of LBP subjects has been seen by Langevin (2009). As mentioned before, a later ultrasound study using elastography found decreased shear strain in the pTLF by inducing flexion using a motorized table (Langevin et al., 2011).

CHAPTER 2

METHODS

This thesis studies the pTLF using ultrasound imaging. Imaging was conducted at the Veterans Affairs New Jersey Health Care System after Institutional Review Board approval from both the VA and NJIT. Data from two subjects without back pain is used in this thesis. Subject 1 has a BMI of 19.7 and subject 2 has a BMI of 25.7. Data from the third subject could not be analyzed because of too much noise in ultrasound images.

2.1 Ultrasound Machine and Data Acquisition

The ultrasound machine used in this study is the Acuson Sequoia C512. A linear array transducer (5-17 MHz), or probe, was used to take B mode video clips while weights were applied. Frequency was set at 15 MHz because this offered the best resolution for the depth we had specified (45 mm). At 45 mm, we are able to see skin, superficial fascia, pTLF, and parts of the underlying paraspinal muscle. Gain was only adjusted if muscle was not clearly seen.

A force transducer can be used to record force measurements in biomechanical testing. A custom made weight holder was used to apply fixed known forces to the probe (see Figure 2.1). A clamp was printed using NJIT's 3D printer. This clamps fits around the narrow part of the probe. Screws are used to hold both clamps together. Threaded beams were attached to clamp and a foam or plastic holder is placed on top in order to hold the weights. The force from any weights placed in this holder is directly transmitted to the probe. The probe and the plastic holder have their own weights which are added to

the total weight applied. Because the user can unintentionally apply his/her own force to the probe while taking images, the probe was held in a foam box in order to stabilize it. Therefore, it does not need to be held.

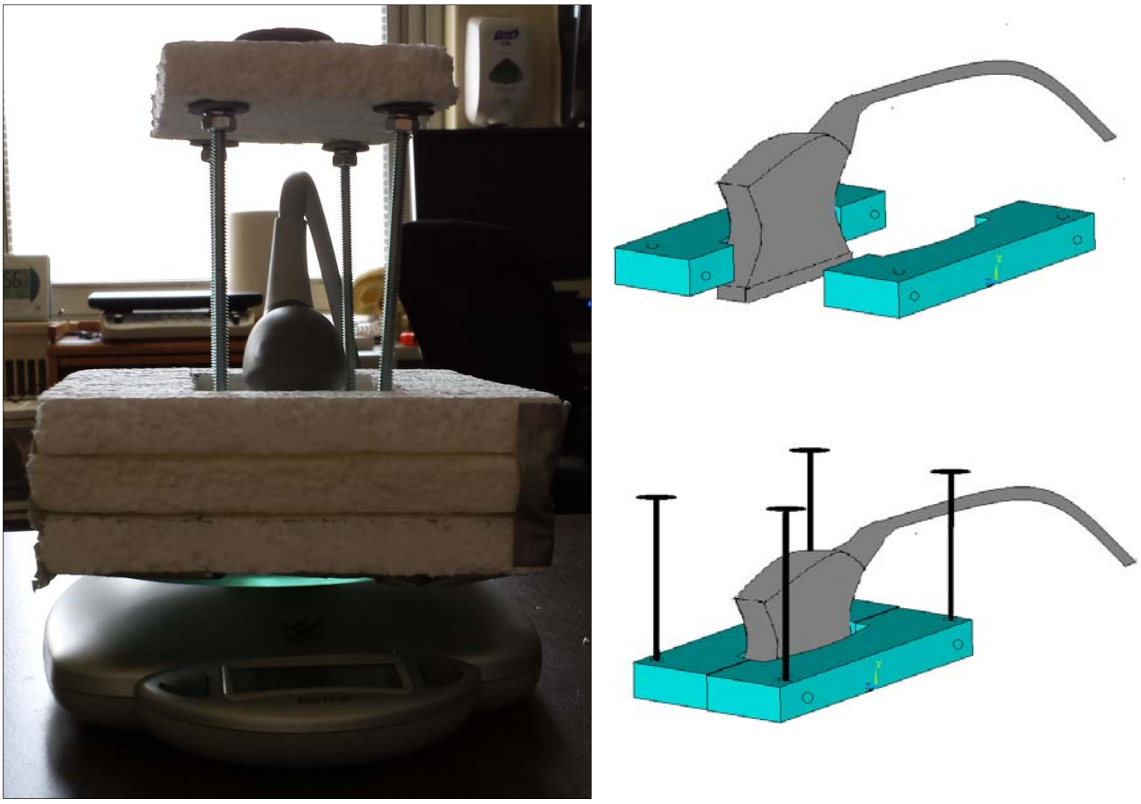

Figure 2.1 The ultrasound probe is held in a foam block which is attached to the body via velcro straps (not seen here). The thredded beams screw into the clamp (right bottom) that is attached to the probe and holds the foam piece with weights. Later, a plastic holder was used.

Ultrasound imaging was done on an area two centimeters lateral to the L2/L3 vertebrae because ultrasound imaging of the thoracolumbar fascia has previously been done here (Langevin 2009, 2011). This is also an area where the fascial plane is most parallel to the skin. At this level, the 2nd layer of the superficial lamina of the pTLF is still visible and the loose connective tissue layer in between is also distinguishable. The L2 vertebra was first located using the 12th rib as a reference point to find T12. Using

palpation, L2 and L3 were then located. A ruler was used to measure 2 cm to right of L2 and a line was drawn parallel to the vertebrae. The probe was aligned along this line.

The subject is asked to like prone on a bed. Once the weight holder is set up, weights are added to the weight holder. Video clips start before weights are added and end a few seconds after the weight is added. This results in an approximately 15 second video clip, sampled at 11 Hz. First, a baseline recording is taken when no weights are applied. Weights are then added in increments of 1 to 4 oz from 1oz to 54 oz. However, if a video clip is too noisy because of subject movement, then it is disregarded. The entire procedure lasts approximately 1 hr.

2.2 Image Processing

All video clips were imported into MATLAB, (Natick, MA). A labeled diagram of a typical frame is seen in figure 2.2.

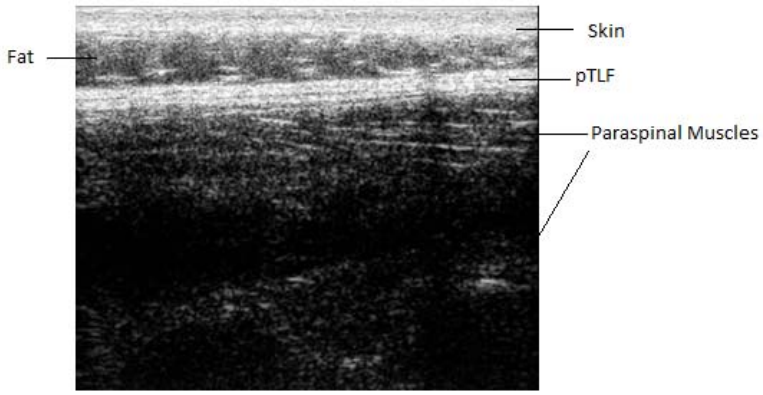

Figure 2.2 A sample ultrasound image is shown here. Bright areas represent hyperechoic areas like skin and fascia while more hypoechoic regions, like fat, are darker. However, the hyperechoic lines in the fat layer may represent the retinacula septas in fat. Muscle fibers can also be seen in the muscle region as hyperechoic lines.

Figure 2.3. This is a magnified image of the skin layer only.

The Matlab script is found in Appendix A. Edge detection software can be used in image processing, but because of a significant amount and intensity of noise found around the borders of each layer in ultrasound imaging, each layer had to be analyzed separately. The algorithm was verified by manually taking comparison measurements in ImageJ (Rasband, 1997)) at various frames. Because there is more noise in the image when applying compression, each frame if first filtered. This is done by converting the image to a gray scale image and then applying a cutoff pixel value so that pixels under this value are set equal to zero. The cutoff pixel value changes in each frame to accommodate the brighter pixels values being seen during compression. In order to measure skin thickness, the image is cropped so that only the skin layer and parts of fat layer remain (Figure 2.3). Since there is a lot of "noise" beneath the skin layer, the 'imfill' function (fills in holes of an image) cannot be used here. Therefore, the location of brightest pixels in each column of the image is determined. Although the noise under the skin layer has pixels of greater value (whiter in color), the intensity of these pixels is less and can be determined by their gray scale value. The border is considered to be an area where the brightest pixels are located. The 'trapz' function is used to find the area below this border which is then divided by the length of the image.

Figure 2.4 Only the deep fascia layer is seen here. The skin above has been cropped out and the image has been converted to a binary image after increasing contrast.

In order to measure thickness of the fat layer, the top border of fascia needs to be determined first (see Figure 2.4). The image is cropped so that the skin layer is no longer seen. It is converted to a binary image using the 'im2bw' function. This function allows the user to set a tolerance which determines which pixels will be given values of 1 or 0. This tolerance has to be changed according to each subject, but can stay the same within each video clip of the same subject as long as the gain was not changed between video clips. In each column of the image, the algorithm searches for a group of pixels with a value of one. A minimum of the group size is set so that noise in the fat layer is ignored. The first pixel in this group represents the top edge of fascia in each column of the image. This value is subtracted from the bottom edge of the skin layer in the same column so that the thickness of the fat layer can be calculated. The same theory is applied to finding the bottom edge of fascia. However, the 'for loop' works backwards so that pixels being analyzed are from the bottom of the image and moving upwards. The thickness of fascia is then calculated by subtracting the top edge from the bottom edge. The average thickness of each layer is calculated by dividing the fat and fascia thicknesses in each column of the image by the length of the image.

In order to analyze the deformation seen in muscle, a different approach has to be taken. The resolution in the muscle layer is quite low because it is at a lower depth. There is also a hypoechoic layer in between the muscle layer (see Figure 2.2). Since the

entire muscle cannot be seen at a depth of 45 mm, the entire thickness of the muscle group is not calculated. Instead, the movement of one muscle edge is tracked to determine the deformation in the muscle layer (see yellow line in Figure 2.5). Figure 2.5a shows a frame with no compression while Figure 25b shows a frame with compression. The yellow line is the edge that needs to be tracked. The increase in intensity is also evident by comparing these two images.

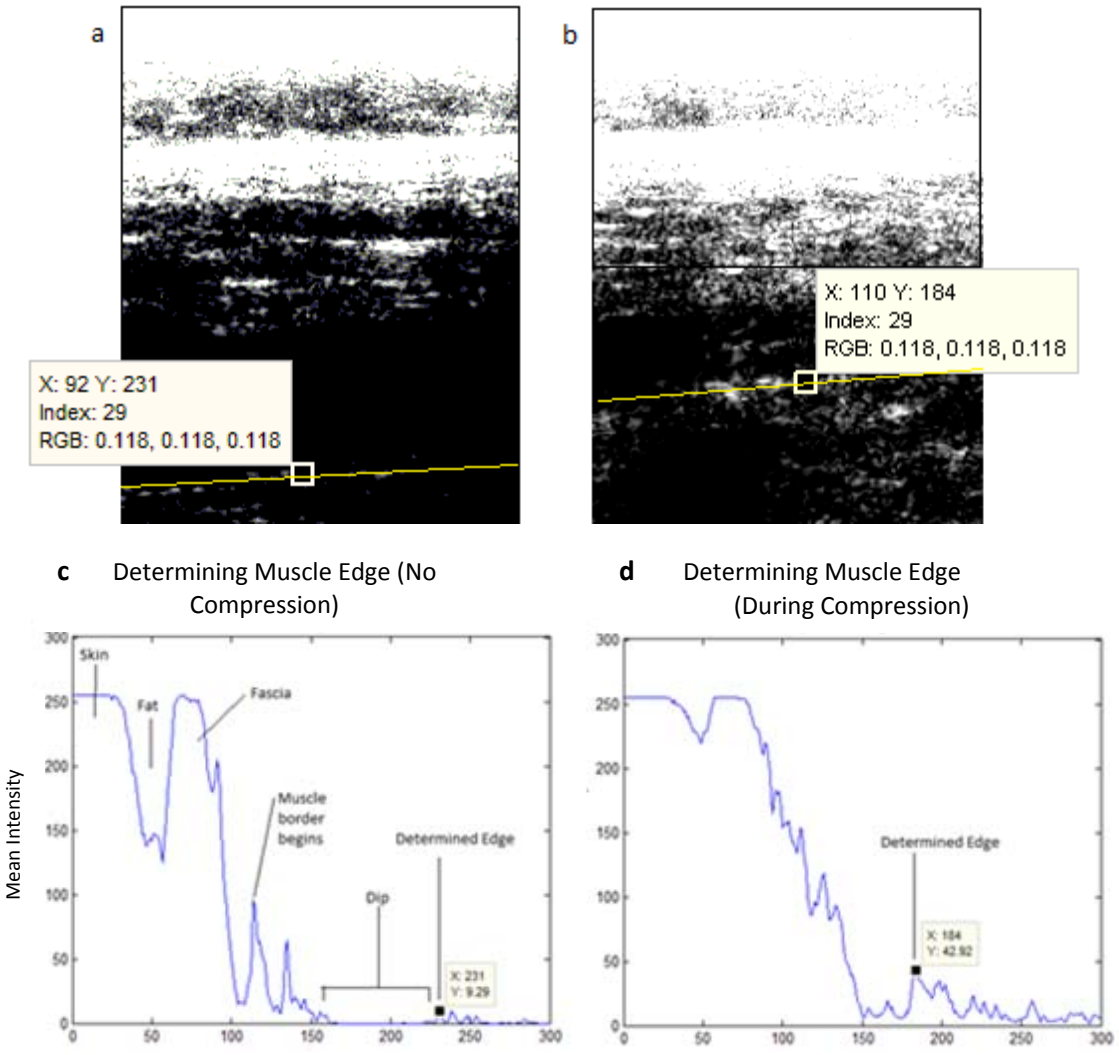

Figure 2.5 a, b,c,d Ultrasound images of no compression *vs* compression are seen in (a) and (b). Plots showing how the Matlab algorithm determines the edge of muscle in the corresponding ultrasound image are seen in (c) and (d).

Figure 2.5c and Figure 2.5d show the plots that determine the edge point. The first peak after a dip in intensity is taken as the beginning of the muscle layer.

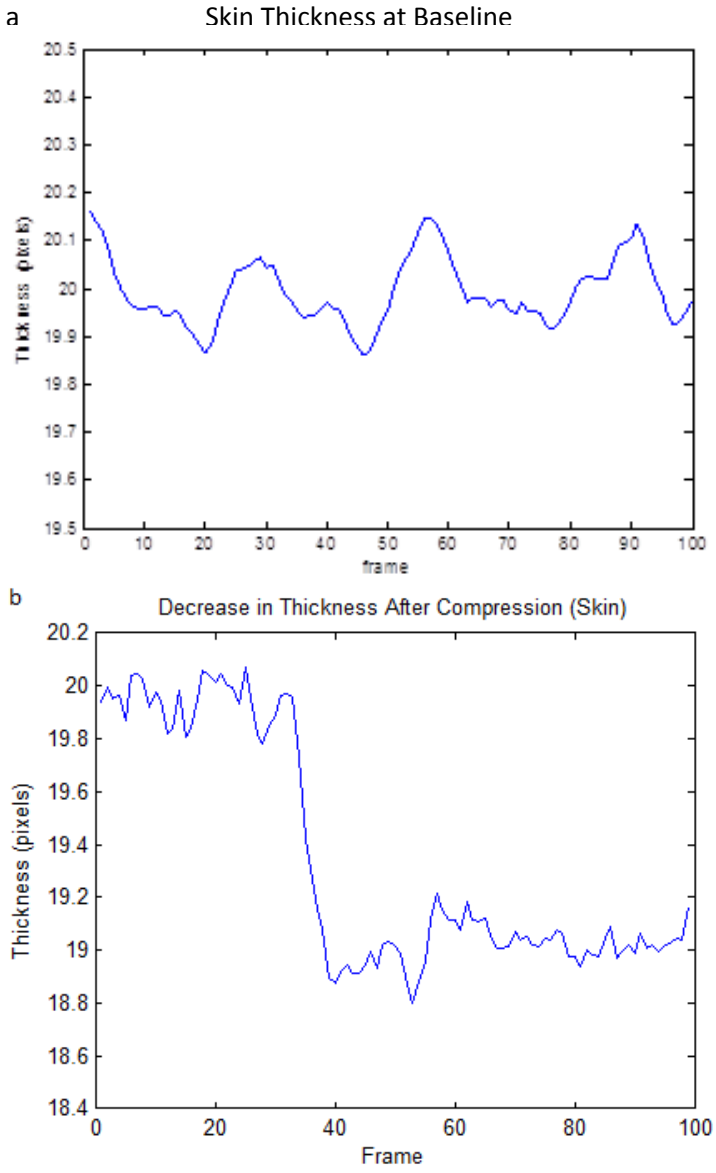

Figure 2.6 a,b Thickness measurements (in pixels) are taken at baseline (a) and after compression (b). During compression the lowest peak is averaged with the values of from the next 20 frames to include the effects of respiration.

Measurements are taken in pixels and then converted to meters. One centimeter is approximately 72 pixels. An example of tracking thickness changes in the skin layer is seen in Figure 2.6a and Figure 2.6.b. The oscillations seen are a result of respirations.

Approximately 3.5 breaths are seen over a range of 9.09 seconds (100 frames). This is an average of 23 breaths per minute. Although this is a high respiratory rate for the average adult, baseline videos were manually analyzed to verify that oscillation are actually due to respirations. The change in thickness measurfed in pixels is very small as seen in these figures. This shows that the algorithm is able to capture even slight changes in thickness. However, respiration thickness changes may affect the measured thicknesses during compression. In the skin and fascia layers, this error may be up to 19% in subject 1 and 12% in subject 2. Since the thickness over 20 frames is averaged when taking the compression thickness, the error due to respiration is decreased.

2.3 Mathematical Models

2.3.1 3D Mathematical Model for Soft Tissue Deformation

As previously stated, manual therapies apply different types of forces including compression, tension, and shear. According to the literature, compressive forces may also be seen during normal physiological changes such as flexion and respirations. This thesis uses a 3D mathematical model (Chaudhry et al., 2008) to determine mechanical constants that can describe the deformation of fascia under applied forces that cause shear, elongation, and compression along different axes. Because soft biological tissues are viscoelastic and stiffen under increased strain, their stress- strain curves are considered non-linear. The nonlinear theory of elasticity is implemented in the mathematic model to incorporates this non-linear characteristic. With the data available, UI tracking can only be done in the vertical direction. The model is applied to a uniaxial

compressive force. The fascia is modeled as one layered, elastic, and isotropic, and like most soft biological tissues, incompressible. Figure 2.7 shows a diagram of the model.

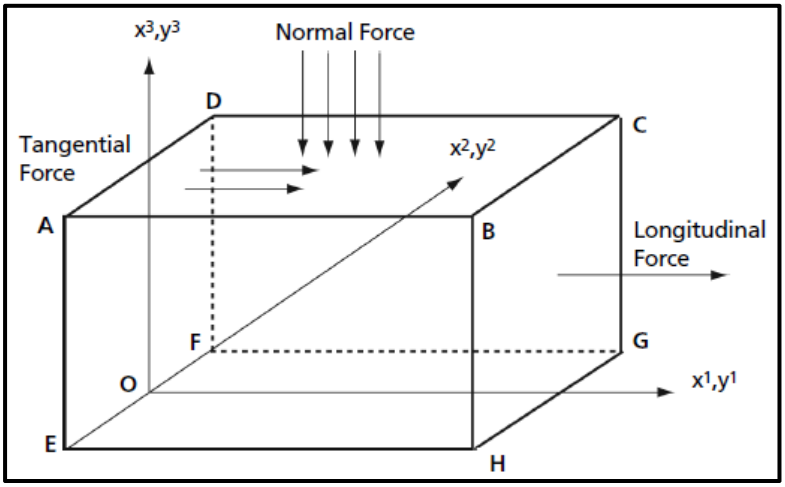

Figure 2.7 The three dimension model used in this mathematical model is show here. Face ABCD is subjected to a normal compressive force.
Source: Chaudhry, Hans, et al. "Three-dimensional mathematical model for deformation of human fasciae in manual therapy." *JAOA: Journal of the American Osteopathic Association* 108.8 (2008): 379-390.

During fascial manipulation, there will be shear and elongation along the x1 axis, extension of the x2 axis, and compression on the x3 axis. x1,x2,x3 represent the undeformed state in each axis and y1,y2,y3 represent the deformed states in each axis. Deformation along each axis is then given by:

$$y1= x1 +k1*x3 +k4*x1 \qquad y2=k2*x3 \qquad y3=k3*x3 \qquad (2.1)$$

where k1 represents the shear ratio from tangential force. k2 represents the extension ratio from compression due to normal force. k3 represents compression ratio from normal force. k4 represents extension ratio from longitudinal force. Because no longitudinal force is applied in this model, k1,k4 = 0.

Metric tensor matrices are used to relate stress and strain in a coordinate system. In a reduced form, the metric tensors in an undeformed state are represented by g_{ij} and g^{ij}; in the deformed state they are represented by G_{ij} and G^{ij}. I,j = 1,2,3 for each axis and r=1,2,3 and represents the summation over r. $g=\left|g_{ij}\right|$, or the determinant of matrix g_{ij} and is equal to 1. $G = \left|G_{ij}\right|$. g_{ij} is the covariant tensor and g^{ij} is the contravariant tensor. g_{ij} and g^{ij} are equal in Cartesian coordinates, but are different in curvilinear (cylindrical, spherical) coordinates. Since Cartesian coordinates are used here, g_{ij} and g^{ij} are equal to each other. Similarly, the deformed state metric tensors, G_{ij} and G^{ij}, are also equal to each other. The metric tensors are defined as the following:

$$g_{ij}=\frac{dx^r*dx^r}{dx^i*dx^j} \qquad g^{ij}=\frac{dx^i*dx^j}{dx^r*dx^r} \qquad G_{ij}=\frac{dy^r*dy^r}{dy^i*dy^j} \qquad G^{ij}=\frac{dy^i*dy^j}{dyx^r*dy^r} \quad (2.2)$$

The strain invariants, I_1, I_2, and I_3, defined below, do not vary whatever coordinate system is used.

$$I_1 = g^{rs}*G_{rs} = {k_1}^2 + {k_3}^2 + {k_2}^2 + (1 + k_4)^2$$

$$I_2 = g_{rs}*G^{rs}=\frac{{k_3}^2+{k_1}^2}{(1+k_4)^2+{k_3}^2}$$

$$I_3 = \frac{G}{g} = 1^* \quad (2.3)$$

The tensor Bij needed to evaluate stress is given by $Bij = I_1 g^{ij} - g^{ir} g^{js} G_{rs}$. The stress produced on the fascia is represented by:

$$\tau^{ij} = \varphi g^{ij} + \psi B^{ij} + pG^{ij}$$

---

[*] Fascia is considered incompressible, so I_3 is set to equal 1. Then, $k_2=\frac{1}{k_3(1+k_4)}$.

where $\varphi = 2\frac{dW}{dI_1}$, $\psi = 2\frac{dW}{dI_2}$, and $p = 2\frac{dW}{dI_3}$

W is the strain energy function for soft tissues described by Demiray (1976) .

$$W = C_1[e^{c_2(I_1-3)} - 1] \tag{2.4}$$

$$\text{So, } \varphi = 2C_1C_2e^{c_2(I_1-3)} \text{ and } \psi = 2\frac{dW}{dI_2} = 0 \tag{2.5}$$

C_1 and C_2 are mechanical constants that need to be determined. C_1 is analogous to the modulus of elasticity and C_2 is a dimensionless constant. In this model, τ^{33} is only considered because there is only compression.

$$\tau^{33} = \varphi g^{33} + \psi B^{33} + pG^{33} \tag{2.6}$$

Chaudhry (2008) finds that $p = -(\varphi + 2\psi)$. Using equations (2.2), (2.3), and (2.4), τ^{33} reduces to:

$$\tau^{33} = \varphi\left(1 - \frac{1}{{k_3}^2}\right) + \psi[(1 + k_4)^2 + {k_2}^2 - \frac{2}{{k_2}^2} \tag{2.7}$$

The normal force that acts on face ABCD (Figure 2.7) can be written as:

$$N = {k_3}^2\tau^{33} \tag{2.8}$$

Using equation (2.5) and (2.7), normal stress is given by:

$$N = 2\left({k_3}^2 - 1\right)C_1C_2e^{c_2(I_1-3)} \tag{2.9}$$

2.3.2 Relationship between Model and Modulus of Elasticity

Because soft tissues materials such as fascia are of nonlinear character, the nonlinear theory of elasticity was used. However, the modulus of elasticity, E, for many tissues is still reported by taking the slope of an initial relatively linear region or a single point in the region where strain is less than 10%. Green's strain, $\frac{1}{2}\left({k_3}^2 - 1\right)$, can be used to evaluate strain at both large and small strains (Fung, 1993). Using (3.9) and Green's strain tensor, E in relation to C_1 and C_2 can be calculated. Both sides of the equation in 2.9 are divided by Green's strain because stress divided by strain is equal to the modulus of elasticity. The following equation is then formed to relate C_1 and C_2 to the modulus of elasticity.

$$\mathrm{E} = 4C_1C_2e^{C_2(I-3)} \tag{2.10}$$

2.3.3 Applying Model to *In Vivo* Setting

The setting under which fascia is being studied must be considered in the above equations. With skin and fat layers above and a muscle layer below fascia, the stress and resulting deformation of fascia will be different in comparison to applying a force directly on fascia. Using equation (2.9) alone does not consider its in vivo setting. Thus, equation 2.9 is changed to:

$$N_t = 2C_{1f}C_{f2}\left({k_{f3}}^2 - 1\right)e^{c_{2f}\left(I_{f1}-3\right)}) \quad (2.11)$$

where N_t stands for theoretical stress, and k_{f3} and I_{f1} are the stretch ratio and first strain invariant of fascia, respectively. The calculated values of C_{1f} and C_{2f} then describe the stress and deformation of fascia when it is in an in vivo setting (below skin and fat and above muscle). Equation (2.10) now becomes

$$E_t=4C_{1f}C_{2f}e^{C_2(I_{f1}-3)} \quad (2.12)$$

The same theory applies in order to calculate experimental E, E_e. Finite element analysis using a linear, elastic, anisotropic model was used to determine E_e (experimental E) of fascia from experimental stress and strain data of all layers at one load that caused strain below 10%. The transverse process of the vertebrae that lies anterior to the muscle is considered to be the boundary condition, although it does not extend down the entire muscle. The model is simplified to a four element model with five nodes. The fifth node is considered the boundary condition where there is no displacement. Each layer is modeled by Hooke's Law, F=kx, where F is the applied force, k is the stiffness of a matrix, and x is the displacement resulting from a certain pressure. Displacement is described as u2-u1. It is derived as seen below:

To=AD
Tn= A'D'

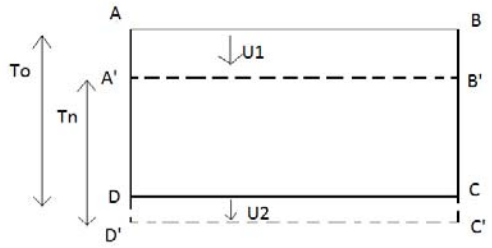

Tn- To = A'D' – AD
= [AD + DD' – u1] – AD
= DD'- u1
= u2- u1

Extending this to each layer, five equations are derived to describe each layer:

a. F- k1(u2-u1) = 0

b. k1(u2-u1) – k2(u3-u2) = 0

c. k2(u3-u2) – k3(u4-u3) = 0

d. k2(u4-u3) – k4(u5-u4) = 0

e. k4(u5-u4) = 0

F stands for the force applied. k1 is the stiffness of skin; k2 is the stiffness of fat; k3 is the stiffness of fascia, and k4 is the stiffness of the underlying muscle group. The values of ui – uj (i,j = 1,2,3,4,5) represent the displacement of each layer and are calculated from new thickness – original thickness for each layer. In this model, a force of 7.4 N and 8.6N is used for subject 1 and subject 2, respectively. This point is taken because it causes less than 10% deformation in all the layers (muscle for subject 2 is an exception—see Figure 3.2b). . This corresponds to the third data point. Using these equations, k1, k2, k3, and k4 are solved for and then used in the following equation to determine Ee.

$$Ee = k*L/ A \qquad 2.13$$

k represents the stiffness of each layer. L represents the thickness of each layer and A represents the area over which pressure was applied which is the area of the bottom of the probe.

The compression ratio, k3 = $\frac{y3}{x3}$ is equal to $\frac{new\ thickness}{original\ thickness}$. Using the data from ultrasound image analysis, the original thickness is calculated by taking the average of the maximum peaks found in the baseline recording. New thickness is recorded by taking the average of 20 frames after the thickness measurements have reached a minimum value for each recording. Experimental stress and experimental compression ratio, k_3, are used to calculate C_1 and C_2 using a least squares regression of the stress-strain curve (see Appendix C for derivation of regression equation). The equations presented above are given in reference to fascia. However, they can be applied to each layer. Results are given for skin, subcutaneous fat ('fat'), posterior layer of TLF ('pTLF'), and the underlying erector spinae muscle grouped as 'muscle'.

CHAPTER 3

RESULTS

Table 4.1 shows the thickness of each layer without compression as calculated by the Matlab code. Langevin (2009) took measurements of the combined fat and pTLF layer and found a mean thickness of .825 cm in subjects without back pain. A combined fat and pTLF thickness for subject 1 is .802 cm and for subject 2 is .752 cm. So, results shown here are similar to Langevin (2009). There are no cadaver studies for comparison that have taken thickness measurements along the midline of the back. Table 4.1 shows that the skin thickness of subject 2 is approximately twice the skin thickness in subject 1. Although subject 2 has a much higher BMI (25.7) than subject 1 (19.5), the fat layer in subject 2 is lower than that of subject 1.

Table 3.1 Thickness of Each Layer at Baseline Measurement

	Subject 1	Subject 2
Skin	.291 cm	.466 cm
Fat	.472 cm	.372 cm
pTLF	.330 cm	.38 cm

Table 3.2 shows determined C_1 and C_2 constants for each subject as well as the theoretical estimate of the modulus of elasticity, E_t. These values are calculated for each layer considered. For both subject 1 and subject 2, the theoretical modulus of elasticity, E_t, are greatest in the skin and pTLF layers. Subject 2's E_t value for skin is much higher that all other layers. This may be a result of having a skin thickness twice as thick as that of subject 1.

Table 3.2 Results for C_1, C_2, and Et for Skin, Fat, pTLF, and Muscle

	Subject 1			Subject 2		
	C_1 (pascals)	C_2 (unitless)	E_t (pascals)	C_1 (pascals)	C_2 (unitless)	E_t (pascals)
Skin	1.1e4	6.6	2.94e5	1.78e5	.8	5.71e5
Fat	0.75e4	3.5	1.22e5	2.4e5	.32	.384e5
pTLF	2.9e4	2.5	2.91e5	0.41e5	.9	1.48e5
Muscle	1.78e4	1.5	1.10e5	0.25e5	.9	.936e5

Table 3.3 shows E_e derived from experimental data using a four element FEM model. It is compared to results found in other studies. For both subject 1 and subject 2, Ee values for skin and pTLF are the highest. E_t values for both subject 1 and subject 2 are repeated here to show a comparison between the mathematical model and the FEM model. Similarity are seen in the skin, fat, and pTLF layers of both subject 1 and 2. A larger difference is seen in the paraspinal muscle group.

Table 3.3 Experimental Modulus of Elasticity for Each Layer

	Estimated E from FEM (subject 1) (Pascals)	Et (subject 1) (pascals)	Estimated E from FEM (subject 2) (Pascals)	Et (subject 2) (pascals)	E from selected studies (Pascals)
Skin	5.44e5	2.94e5	5.76e5	5.71e5	~5e3 ~ 2e6
Subcutaneous Fat/ Superficial Fascia	1.14e5	1.22e5	.388e5	.384e5	~3.9e3
pTLF	7.88e5	2.91e5	2.72e5	1.48e5	Not available
Paraspinal Muscle Group	1.33e4	1.10e5	.915e4	.936e5	~5e4 to ~9e4

Tables 3.4 and 3.5 provide the data calculated by analyzing video clips in Matlab. The thickness of each layer can be seen at a corresponding load (stress). Using these values, displacement from the original thickness can be determined.

Table 3.4 Subject 1 Results

Stress (pascals)	Skin Thickness (m)	Fat Thickness (m)	Fascia Thickness (m)	Muscle Thickness (m)
0	0.002809	0.004715	0.0033017	0.0358333
10731.8	0.0027596	0.004436	0.0032549	0.03416
11160.6	0.0027518	0.004254	0.0032549	0.03305
11589.3	0.0027229	0.004254	0.0032191	0.03194
12446.9	0.0027229	0.004179	0.0031985	0.031527
13304.5	0.0026638	0.004139	0.0031600	0.0311111
17163.6	0.0026283	0.004122	0.0031586	0.0306944
20593.9	0.0026079	0.004043	0.0031105	0.030277
22309.0	0.0026047	0.004030	0.0031036	0.029861
23595.4	0.0026016	0.004008	0.0030474	0.029722
29169.6	0.0025828	0.003952	0.0029801	0.028472
32600.0	0.0025795	0.003918	0.0029361	0.027638
36030.3	0.0025555	0.003873	0.0029019	0.027222
37745.4	0.0025138	0.003696	0.0028799	0.026666

Table 3.5 Subject 2 Results

Stress (pascals)	Skin Thickness (m)	Fat Thickness (m)	Fascia Thickness (m)	Muscle Thickness (m)
0	0.00466	0.00372	0.0038	0.04166
12446.9	0.00463	0.00323	0.00368	0.03777
12875.7	0.00455	0.00247	0.00363	0.03625
15448.4	0.00454	0.00235	0.00362	0.03611
16734.8	0.00452	0.00219	0.00357	0.03597
18021.2	0.00451	0.00215	0.00349	0.03332
19307.5	0.00448	0.00187	0.00338	0.03305
21451.5	0.00448	0.00182	0.00332	0.03263
25310.6	0.00445	0.00182	0.00319	0.03180
27454.5	0.00442	0.00168	0.00307	0.03125

Figure 3.1 a and 3.1 b show the theoretical fit (solid curve) for experimental data (circles) of skin for subject one and subject two.

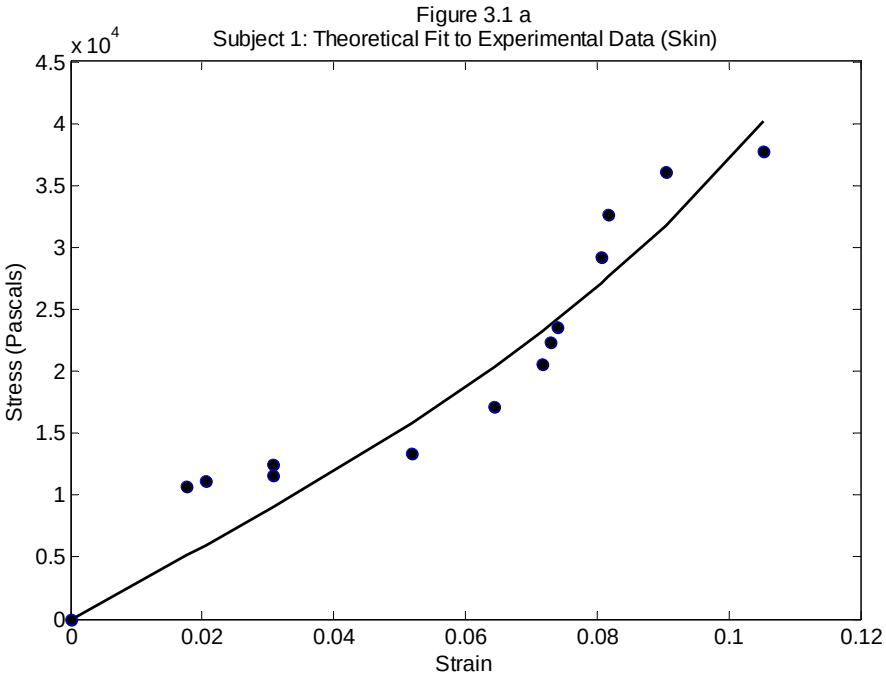

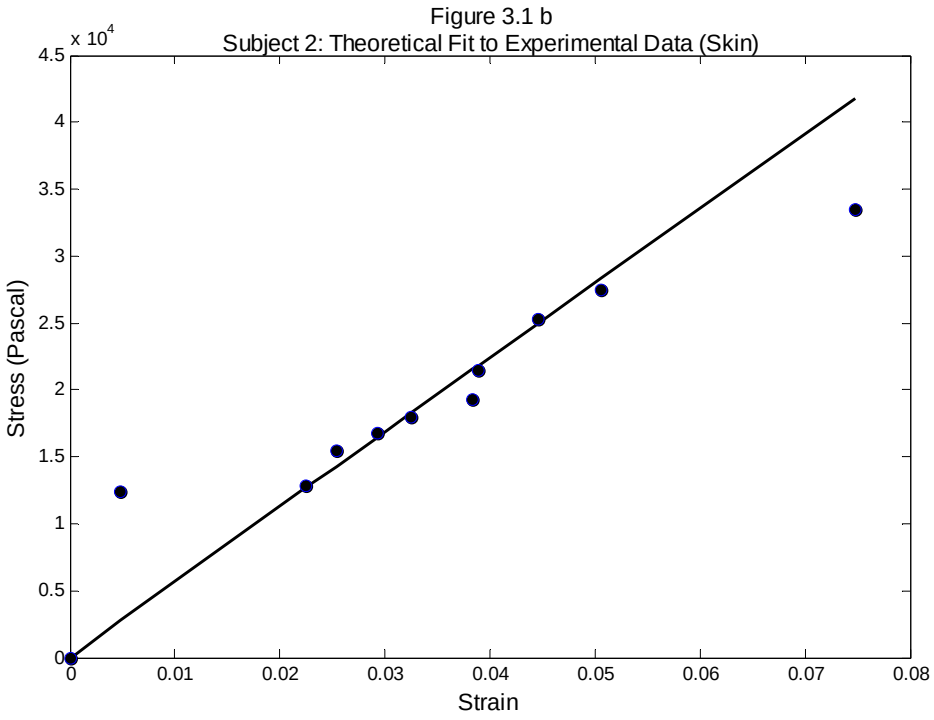

Figure 3.1 a, b Experimental and Theoretical Results for Skin Layer of Subject 1 and 2

Figure 3.2 a and 3.2 b show the theoretical fit (solid curve) for experimental data (circles) of fat for subject one and subject two.

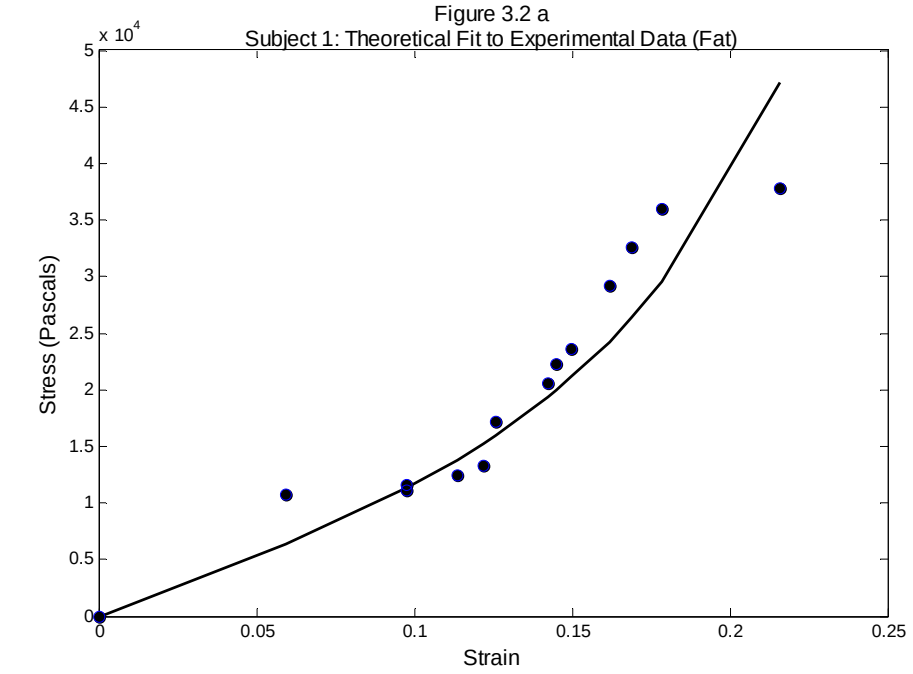

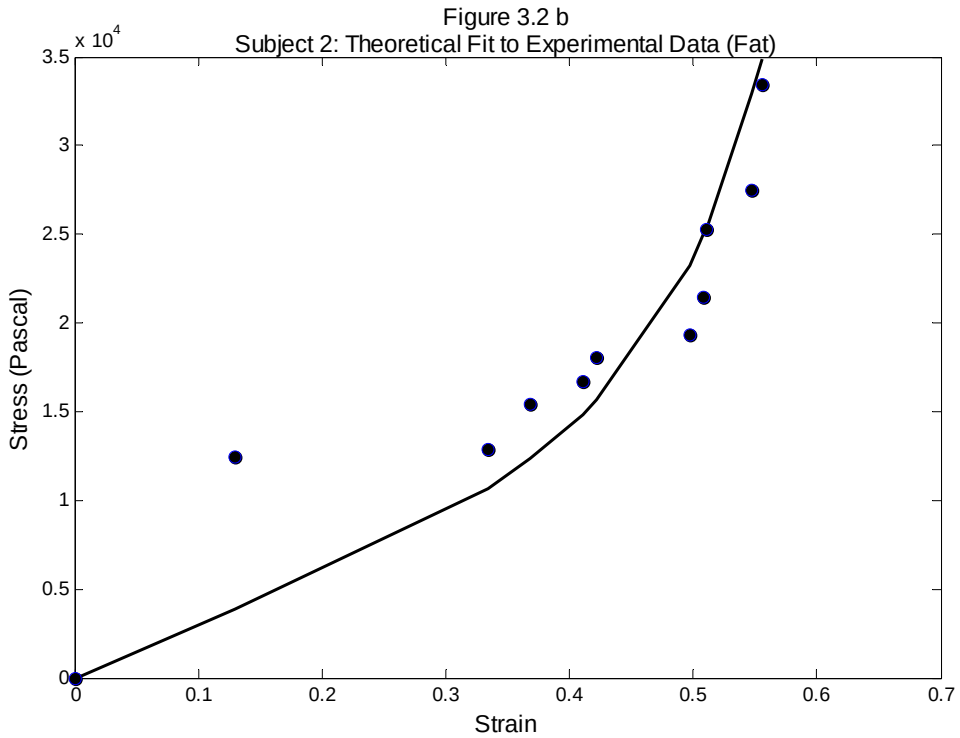

Figure 3.2 a,b Experimental and Theoretical Results for Fat Layer of Subject 1 and 2

Figure 3.3 a and 3.3 b show the theoretical fit (solid curve) for experimental data (circles) of pTLF for subject one and subject two.

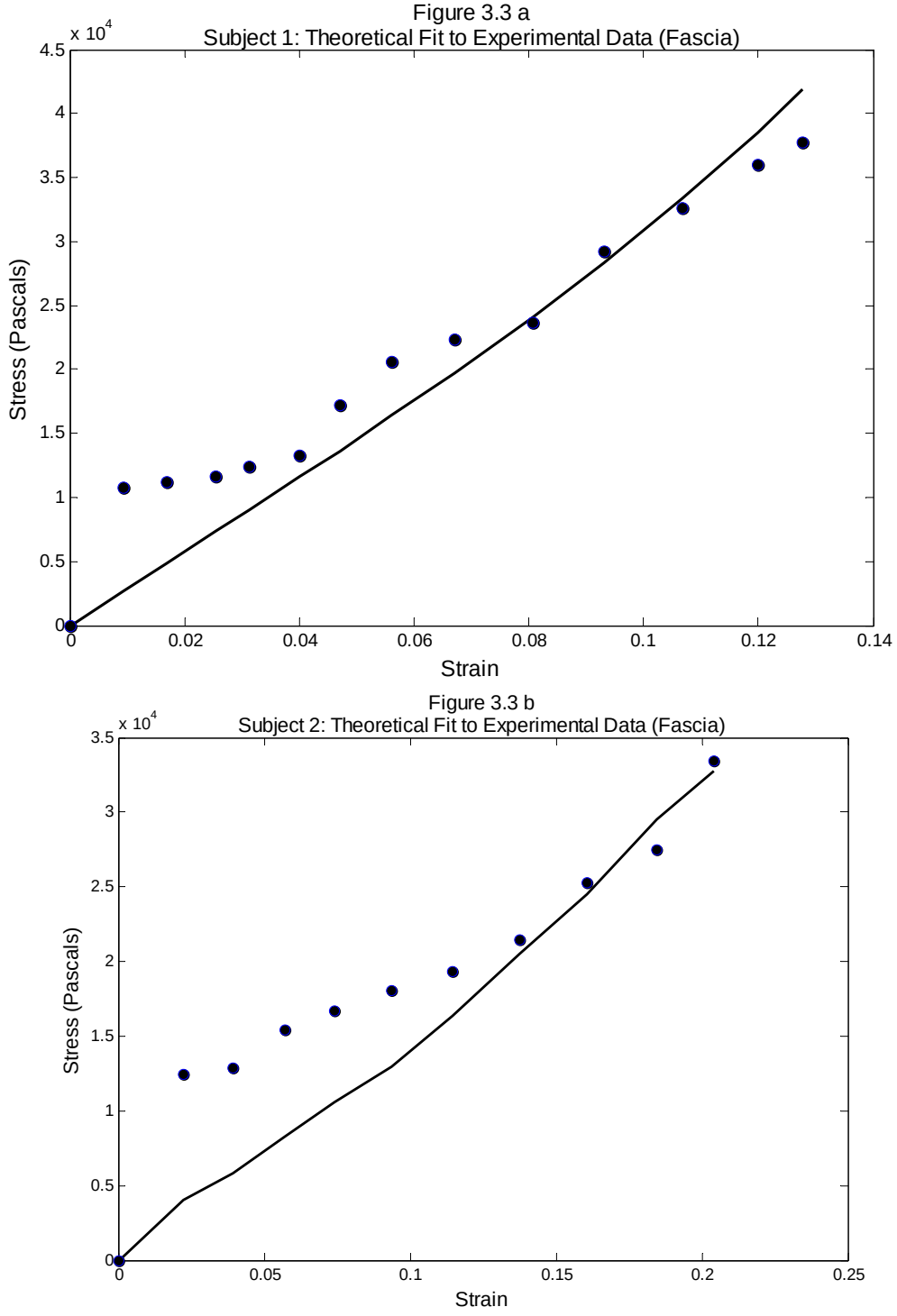

Figure 3.3 a,b Experimental and Theoretical Results for Fat Layer of Subject 1 and 2

Figure 3.4 a and 3.4 b show the theoretical fit (solid curve) for experimental data (circles) of the muscle group for subject one and subject two.

Figure 3.4 a

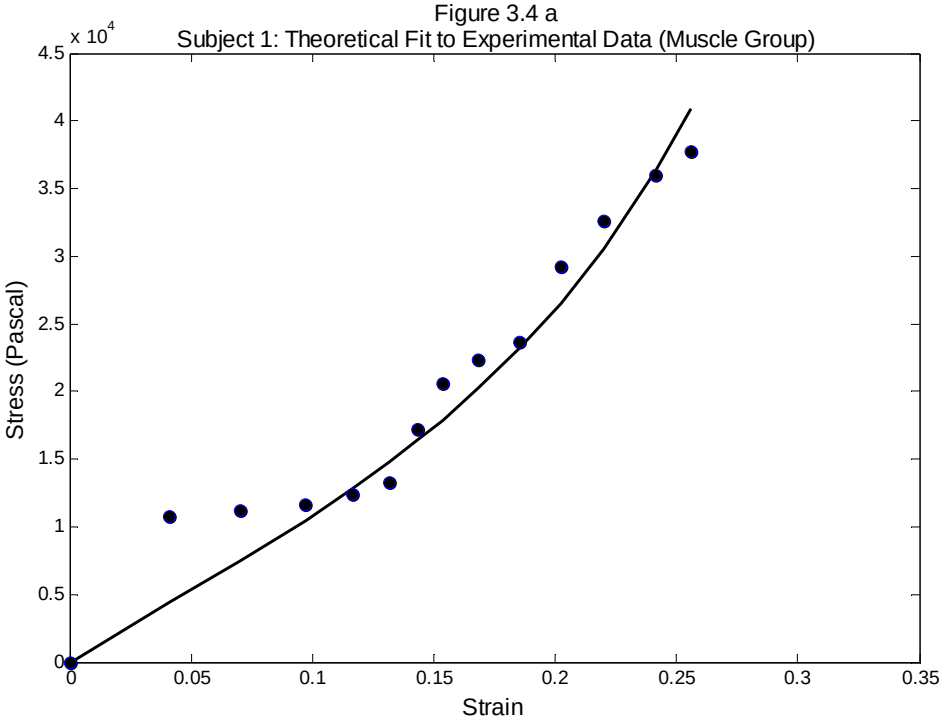

Figure 3.4 b

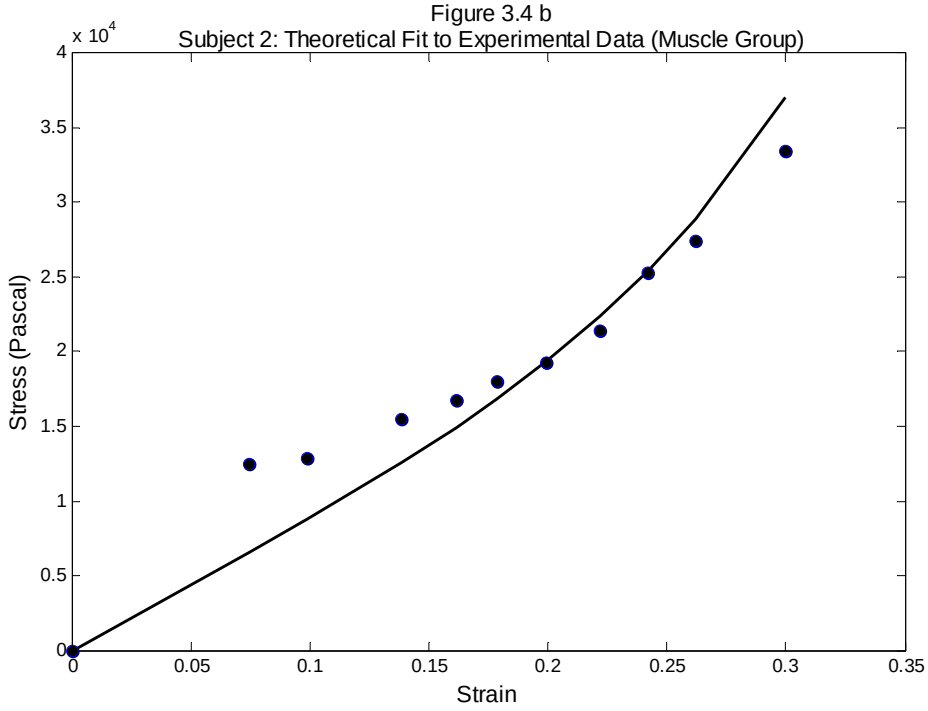

Figure 3.4 a,b Experimental and Theoretical Results for Fat Layer of Subject 1 and 2

CHAPTER 4

DISCUSSION AND CONCLUSION

The goal of this study was to use ultrasound imaging to track deformations seen in fascia under known compressive forces. Although ultrasound imaging is widely used in a clinical setting, the best way to quantitatively analyze the various types of ultrasound data is still under scrutiny. Here, B mode images were used to track changes in thickness. Figure 3.3a and 3.3b shows that the algorithm here is sensitive to very small changes. However, accuracy of this algorithm must first be determined because it shows changes on an order of less than one pixel. Since a pixel is the smallest unit of length in an image, the algorithm is detecting a change of more than one pixel, but is then divided by the length of the image in order to calculate the average thickness. Measuring accuracy of ultrasound measurements is usually done using phantoms with known elastic properties. A gelatin phantom was created early in the study to create a preliminary image tracking code. However, its elastic properties could not be determined with enough accuracy to compare to ultrasound images.

The non-linear mathematical model used here (Chaudhry et al., 2008) was originally tested for *in vitro* fascia treated as an isolated layer. However, in an *in vivo* setting, all the layers above and below fascia must be considered. Table 4.2 and Table 4.3 shows results for all layers considered in this setting. C_1 values for subject 1were lower than C_1 values for subject 2 while C_2 values for subject 2 were greater. However, their Et and Ee values are similar. This shows that C_1 and C_2 not only represent the stress-strain curve in the linear region where the modulus of elasticity is usually

measured; but, it can also describe the response over a larger stress range. For example, when applying manual therapy, a force as great as 100 N has been observed (Chaudhry et al., 2008). The stiffness at higher forces cannot be measured using only the modulus of elasticity. Thus, C_1 and C_2 can act as mechanical constants to describe any type of viscoelastic tissue over a large range of stresses.

E_t values are similar to E_e results calculated from a finite element model. The differences between these two values is attributed to how close the theoretical curve is to the experimental data at the point considered in FEM. Displacement at the third stress point was measured for each layer in the FEM model. If the theoretical curve at this point is closer to the experimental point, then E_t and E_e values are more similar. This can be seen by comparing values in Table 1 and Table 2. For example, E_t and E_e values for fat in both subject 1 and 2 are close because the data points fall on or close to the theoretical curve. For fascia in both subjects, the third data point is further away from the theoretical curve and therefore, a greater difference between E_t and E_e is seen.

Figure 4.3a and 4.3b show the theoretical curves that describe fascia *in vivo*. There are larger errors towards the beginning and end of the curves. Error seen in the beginning of the curve may be due to an inadequate number of data points. The probe's weight causes significant strain so that smaller strains cannot be recorded. This is especially evident in subject 2's fat layer data (Figure 4.2b). Baseline data is taken when the probe is applying the least possible pressure. However, it is possible that this method of baseline measurement is inadequate. Using a modified force transducer is essential for more accurate force measurements.

Figure 3.3a and 3.3b show a change in thickness resulting from increasing intra-abdominal pressure during respiration. An increase in stiffness would not allow normal movement of the fascia as well as the underlying muscles. Furthermore, this stiffness can be tracked in a clinical setting using C_1 and C_2. For example, it can be used to track stiffness of fascia before and after manual therapy to determine progress of myofascial release treatments. Patients with plantar fasciitis may undergo a plantar fasciotomy, which is the cutting of fascia found at the bottom of the foot, to relieve increased tension. However, as discussed in Chapter 1, fasciae are an important source of force transmission; cutting fascia will not only disrupt force transmission, but decrease the efficiency of muscles in its myofascial unit. Manual therapy aimed at decreasing the tension in this fascia is an alternative. Another clinical application of tissue stiffness measurements has recently been studied in the field of cancer research. It has been seen that increased stiffness in the extracellular matrix fibers around a tumor promotes cancer growth and metastasis. Thus, determination of stiffness is important in tracking cancer growth. More research into why this relationship exists is currently underway, but quantifiable measurements like C_1 and C_2 that can be used to describe tissue stiffness may aid in discovering this relationship. To correctly implement the model, more data points in the small strain and large strain regions need to be taken. However, the approach described in this thesis may be used as a basis for future studies to build upon.

Future research would try to model the different layers of fascia with greater accuracy. For example, through histological studies, the fiber angle in each collagen layer is known. Using this relationship, future models may incorporate the transduction of force along different directions. Because the loose connective tissue layers give fascia a

viscoelastic behavior, they would need to be modeled in more detail. In people with low back pain, this layer is much thicker and easy to quantify in terms of thickness. Future models may want to consider each layer of fascia separately and with different strain energy functions. Finally, the tensile modulus of elasticity and the shear modulus are also of great importance because fascia faces these types of force more commonly. Using a different type of ultrasound data, these properties should also be measured *in vivo*.

APPENDIX A

IMAGE ANALYSIS MATLAB CODE

Appendix A contains the Matlab code that was used to analyze each video clip. Data is then exported to an excel sheet.

```
clip=VideoReader('clip1a.avi');
nFrames=get(clip,'numberOfFrames');
mov=read(clip);
%Skin layer
for i=1:nFrames;
    frame=read(clip,i);
    framecrop= frame(51:350,100:440,:);  %100:440
    Im= rgb2gray(framecrop);
    skin=Im(1:35,:);
    [r,c,v]=find(skin>235);
    skinborder=[r c];
    h=find(r<16); %may need to change
    skinborder(h,:)=[];
    Sthick(i)=(trapz(skinborder(:,1)))/(length(skinborder));
end

%Fat layer
for j= 1 :nFrames
    frame2=read(clip,j);
    framecrop2=frame2(51:350,100:440,:);
    Im2=rgb2gray(framecrop2);
    bw=Im2(40:150,20:311,:);  %may have to change 40
    m=mean(bw);
    mm(j)=mean(m)+80; %may have to change according to noise level
    [r4,c4]=find(bw< mm(j));
    for o=1:length(r4);bw(r4(o),c4(o))=0;end
    fatlayer=im2bw(bw,.5);   %may have to change


    fatlayer=fatlayer(:,1:100);sizef=size(fatlayer);l=sizef(1,2);
    %changed 10:200 to 1:100;
    ss=size(fatlayer);s(j)=ss(1,1);
    [r2,c2]=find(fatlayer>0);
    b=[r2,c2];
     fatlayer2=im2bw(bw,.2);fatlayer2=imfill(fatlayer2,'holes');
    fatlayer2=fatlayer2(:,94:224); %or1:100
     [r3,c3]=find(fatlayer2>0);
    b2=[r3,c3];
    Im3=imadjust(Im2,[.1 .5],[]);Im5=Im3(:,1:200); % change based on
straightest region?
%     Im4=im2bw(Im3,.5);Im5=imfill(Im4,'holes');

    for k= 1:l  %column by column
            a= find(c2==k);
```

```
            matrix= b(a,:);
            a2=find(c3==k);matrix2=b2(a2,:);
            if length(matrix)==0;matrix=[1 k];end

            for m=1:length(matrix)    %analyze each column
                if length(matrix)==2; first=matrix(1,1); break,end
                first=matrix(m,1);aa=first+10;if first>60;break,end
                bb=fatlayer(first:aa,k);bb=bb+0;
                  if mode(bb)==1, break,end
                  if m==length(matrix),break,end
            end

            edge(k)= matrix(m);%edge gives determined edge point of fsc
               edge(1)=25;
               if edge(k)>30,edge(k)=edge(k-1);end;
            for n= 1:length(matrix2) %loop for fascia
              f=length(matrix2)-n ;
              if f==0;f=1;first2=matrix2(f,1);break,end;
              if length(matrix2)==2,f=1;first2=matrix2(f,1);break,end
                first2=matrix2(f,1);aa2=first2-5;if first2<6,break,end
                bb2=fatlayer2(aa2:first2,k);bb2=bb2+0;
                    if bb2(:,1)==1,break,end
            end

            edge3(k)=first2; %for fascia
                if edge3(k)>60;
                    edge3(k)=edge3(k-1);end
            ct=fatlayer(edge3(k):edge3(k)+15,k);
                h=find(ct>0);le=length(h);if le==0,h=1;le=1;end

                edge5(k)= edge3(k)+ h(le);
                ctlayer=edge5(k)-edge3(k);
            fasciathick(k)=edge5(k)-edge(k);%for fascia
    end

        %muscle tracking
        for v=1:300, row(v)=mean(Im5(v,:));end
        row2=row(1:250);  %may have to change 250 as cut off
        v2=find(row2<40);if size(v2)==[1 0],v2=find(row2<100); end
%may have to change50 as cutoff
        v3=v2(1,1);v4=row2(170:length(row2));
        edge4=find(row2==max(v4)); if
length(edge4)>1;edge4=edge4(:,length(edge4));end
        muscle(j)=edge4;
      edge2=edge+40; %for fat
     fthick=edge2-Sthick(j);fthick2=trapz(fthick);%for fat
           Fthick(j)=fthick2/length(fatlayer); %for fat
      Fasciathick(j)=mean(fasciathick); %for fascia
      Ctlayer(j)=mean(ctlayer);
end
 muscle2=max(muscle)-min(muscle);
subplot(4,1,3);plot(Fasciathick);title('Fascia
Thickness');xlabel('frame');ylabel('pixels');
 subplot(4,1,4);plot(muscle);title('Muscle
Movement');xlabel('frames');ylabel('pixels');
```

APPENDIX B

MATLAB CODE USED TO ANALYZE DATA

Data is imported from an excel sheet and analyzed. The first section imports the data and calculates k3 values for each layer. The second section solves the Finite Element Model. The third section solves for c1 and c2 variables. The fourth section checks c1 and c2 values.

```
clear all
%% stress strain data
h=xlsread('data1');
skin=sort(h(1,:)*5/36/1000;
fat=sort(h(2,:))*5/36/1000;
fascia=sort(h(3,:)*5/36/1000;
muscle=sort(h(4,:)*5/36/1000;
weight=[0 1 2 3 5 7 16 24 28 31 44 52 60 64];
kg=weight*.0283; kg=kg+.62 + .06; kg(1,1)=0; %add ultrasound probe
weight and weight holder weight
force=kg*10;
stress=force/.00066;  %pascals
k3skin=skin/max(skin);
k3fat=fat/max(fat);
k3fascia=fascia/max(fascia);
k3muscle=muscle/max(muscle);

strainskin=abs(k3skin-1);
strainfat=abs(k3fat-1);
strainfascia=abs(k3fascia-1);
strainmuscle=abs(k3muscle-1);

P=1.0732e4*.00066;
delta1=abs((skin(1,2)-skin(1,1)));
delta2=abs((fat(1,2)-fat(1,1)));
delta3=abs((fascia(1,2)-fascia(1,1)));
delta4=abs((muscle(1,2)-muscle(1,1)));
syms k1 k2 k3 k4
eq1=P-k1*(delta1)==0;
eq2=k1*delta1-k2*delta2==0;
eq3=k2*delta2-k3*delta3==0;
eq4=k3*delta3-k4*delta4==0;
S=solve(eq1,eq2,eq3,eq4,k1, k2, k3,k4);
S=[S.k1 S.k2 S.k3 S.k4];
k1=S(1);k2=S(2);k3=S(3);k4=S(4);

%Then use following each equation to solve for E for each layer
E1=k1*skin(1,1)/.00066;
E2=k2*fat(1,1)/.00066;
```

```
E3=k3*fascia(1,1)/.00066;
E4=k4*fascia(1,1)/.00066;

%%
%solve for c1 c2
y=stress;
k3=k3skin;
I=k3.^2 +(1./(k3.^2))+ 1;
syms a b
% eq1= sum(2.*((k3.^2-1).^2).*b.*exp(2.*a.*(I-3))) - sum(y.*exp(a.*(I-
3)).*(k3.^2-1))==0;
% eq2= sum(2.*(k3.^2-1).*b.*exp(a.*(I-3)).*(exp(a.*(I-3)) + a.*(I-
3).*exp(a.*(I-3)))) - sum(y.*(k3.^2-1).*(exp(a.*(I-3)) + a.*(I-
3).*exp(a.*(I-3))))==0;
S2=solve(sum(2.*((k3.^2-1).^2).*b.*exp(2.*a.*(I-3))) -
sum(y.*exp(a.*(I-3)).*(k3.^2-1))==0, sum(2.*(k3.^2-1).*b.*exp(a.*(I-
3)).*(exp(a.*(I-3)) + a.*(I-3).*exp(a.*(I-3)))) - sum(y.*(k3.^2-
1).*(exp(a.*(I-3)) + a.*(I-3).*exp(a.*(I-3))))==0);


 %%
%Check c1 c2
c2=a; c1=b/c2;
N1=2*(k3.^2-1).*c1.*c2.*exp(c2.*(I-3));
plot(strainskin,abs(N1),'g');hold on;plot(strainskin,stress,'o');
Et=4.*c1.*c2*exp(c2*(I-3));
```

APPENDIX C

DERIVATION OF LEAST SQUARES REGRESSION MODEL

Appendix C shows how the least squares regression model was derived.

In a least squares regression, the solution minimizes the sum of the error between two equations. Here, equation 2.11 is used to calculate theoretical stress. The difference between experimental and theoretical stress is minimized.

First derivatives of
S=sum(y – $[2C_{1f}C_{2f}\left(k_{f3}{}^{2}-1\right)e^{c_{2f}\left(I_{f1}-3\right)}]$)^2

y= experimental stress corresponding to each compression ratio
a=C2
b= C1*C2

dS/dC1 = sum(2((k_3^2-1) 2) *b*e $^{(2a\ (I-3))}$) - sum(y*e $^{(a\ (I-3))\ (k_3\text{^}2-1)}$)

dS/dC2= sum(2 (k_3^2-1) *b*e $^{(a(I-3)}$)*(e $^{(a(I-3))}$ + a*(I-3)*e $^{(a.*(I-3))}$)) - sum(y*(k_3^2-1)* (e$^{(a(I-3))}$ + a(I-3)* e $^{(a(I-3))}$))

The derivative of S with respect to C1 and C2 are calculated and then set equal to zero. C1 and C2 are then solved for using the "solve" function in Matlab. This is similar to an objective function. The same theory is applied to skin, fat, and muscle data.

REFERENCES

Adams, M. A., et al. *The biomechanics of back pain*. Edinburgh, Scotland: Churchill Livingstone, 2007.

Agache, P. G., et al. "Mechanical properties and Young's modulus of human skin *in vivo*." *Archives of dermatological research* 269.3 (1980): 221-232.

Barker, P. J., C.A. Briggs, and G. Bogeski. "Tensile transmission across the lumbar fasciae in unembalmed cadavers: effects of tension to various muscular attachments." *Spine* 29.2 (2004): 129-138.

Benetazzo, L., et al. "3D reconstruction of the crural and thoracolumbar fasciae." *Surgical and radiologic anatomy* 33.10 (2011): 855-862.

Benjamin, M. "The fascia of the limbs and back–a review." *Journal of anatomy* 214.1 (2009): 1-18.

Bogduk, N., J. E. Macintosh, and M. J. Pearcy. "A universal model of the lumbar back muscles in the upright position." *Spine* 17.8 (1992): 897-913.

Chaudhry, H., et al. "Three-dimensional mathematical model for deformation of human fasciae in manual therapy." *JAOA: Journal of the American osteopathic association* 108.8 (2008): 379-390.

Corey, S. M., et al. "Sensory innervation of the nonspecialized connective tissues in the low back of the rat." *Cells tissues organs* 194.6 (2011): 521-530.

Demiray, H. "Stresses in ventricular wall." *Journal of applied mechanics* 43 (1976): 194.

Dittrich, R. J. "Lumbrodorsal fascia and related structures as factors in disability." *The Journal-lancet* 83 (1963): 393.

Federative Committee on Anatomical Terminology. *Terminologia anatomica: international anatomical terminology*. Stuggart, Germany: Thieme, 1998.

Fung, Y. C. "Biomechanics: material properties of living tissues." Tokyo, Japan: Springer Japan, 1993.

Gatton, M. L., et al. "A three-dimensional mathematical model of the thoracolumbar fascia and an estimate of its biomechanical effect." *Journal of biomechanics* 43.14 (2010): 2792-2797.

Gerlach, U. J., and W. Lierse. "Functional construction of the superficial and deep fascia system of the lower limb in man." *Cells tissues organs* 139.1 (1990): 11-25.

Gracovetsky, S., H. F. Farfan, and C. Lamy. "A mathematical model of the lumbar spine using an optimized system to control muscles and ligaments." *The orthopedic clinics of north America* 8.1 (1977): 135.

Hijing, P. et al. *Fascia Research II: Basic science and implications for conventional and complementary health care*. Amsterdam, Netherlands: Elsevier, 2009.

Lambertz, D., U. Hoheisel, and S. Mense. "Distribution of synaptic field potentials by TTX-resistant skin and muscle afferents in rat spinal segments L4 and L5." *Neuroscience letters* 409.1 (2006): 14-18.

Lancerotto, L., et al. "Layers of the abdominal wall: anatomical investigation of subcutaneous tissue and superficial fascia." *Surgical and radiologic anatomy* 33.10 (2011): 835-842.

Langevin, H. M., et al. "Ultrasound evidence of altered lumbar connective tissue structure in human subjects with chronic low back pain." *BMC musculoskeletal disorders* 10.1 (2009): 151.

Langevin, H. M., et al. "Reduced thoracolumbar fascia shear strain in human chronic low back pain." *BMC musculoskeletal disorders* 12.1 (2011): 203.

Loram, I. D., C. N. Maganaris, and M. Lakie. "Use of ultrasound to make noninvasive in vivo measurement of continuous changes in human muscle contractile length." *Journal of applied physiology* 100.4 (2006): 1311-1323.

Macintosh, J. E., N. Bogduk, and S. Gracovetsky. "The biomechanics of the thoracolumbar fascia." *Clinical biomechanics* 2.2 (1987): 78-83.

Okotie, G., et al. "Tendon strain measurements with dynamic ultrasound images: evaluation of digital image correlation." *Journal of biomechanical engineering* 134.2 (2012).

Ophir, J., et al. "Elastography: imaging the elastic properties of soft tissues with ultrasound." *Journal of medical ultrasonics* 29.4 (2002): 155-171.

O'Sullivan, P. B., et al. "Lumbar repositioning deficit in a specific low back pain population." *Spine* 28.10 (2003): 1074-1079.

Purslow, P. P. "The structure and functional significance of variations in the connective tissue within muscle." *Comparative biochemistry and physiology-part a: molecular & integrative physiology* 133.4 (2002): 947-966.

Rasband, W.S. (1997) ImageJ (Version 1.47) [software]. Bethesda, Maryland: U.S National Institute of Health. Retrieved from http://imagej.nih.gov/ij/.

Römgens, A. M., C. C. Van Donkelaar, and K. Ito. "Contribution of collagen fibers to the compressive stiffness of cartilaginous tissues."*Biomechanics and modeling in mechanobiology* (2013): 1-11.

Samani, A., J. Zubovits, and D. Plewes. "Elastic moduli of normal and pathological human breast tissues: an inversion-technique-based investigation of 169 samples." *Physics in medicine and biology* 52.6 (2007): 1565.

Schleip, R., et al. "Strain hardening of fascia: Static stretching of dense fibrous connective tissues can induce a temporary stiffness increase accompanied by enhanced matrix hydration." *Journal of bodywork and movement therapies* 16.1 (2012): 94-100.

Smeulders, M., et al. "Spastic muscle properties are affected by length changes of adjacent structures." *Muscle & nerve* 32.2 (2005): 208-215.

Standring S. *Gray's anatomy, the anatomical basis of clinical practice, 40th edn*. Edinburgh, Scotland: Churchill Livingstone, 2008.

Stecco, A., et al. "Pectoral and femoral fasciae: common aspects and regional specializations." *Surgical and radiologic anatomy* 31.1 (2009): 35-42.

Stecco, C., et al. "A histological study of the deep fascia of the upper limb." *Italian journal of anatomy and embryology* 111 (2006): 105-10.

Stecco, C., et al. "Mechanics of crural fascia: from anatomy to constitutive modeling." *Surgical and radiologic anatomy* 31.7 (2009): 523-529.

Stecco, L.. *Fascial manipulation for muscoloskeletal pain*. Padova, Italy: Piccin Nuova Libraria SpA, 2004.

Stecco, L., and C. Stecco. *Fascial manipulation: practical part*. Padova, Italy: Piccin Nuova Libraria SpA, 2009.

Stecco, C., et al. "Tendinous muscular insertions onto the deep fascia of the upper limb. First part: anatomical study." *Morphologie* 91.292 (2007): 29-37.

Taguchi, T., U. Hoheisel, and S. Mense. "Dorsal horn neurons having input from low back structures in rats." *Pain* 138.1 (2008): 119-129.

Tesarz, J., et al. "Sensory innervation of the thoracolumbar fascia in rats and humans." *Neuroscience* 194 (2011): 302-308.

Tesh, K. M., J. S. Dunn, and J. H. Evans. "The abdominal muscles and vertebral stability." *Spine* 12.5 (1987): 501-508.

Tomasek, J., et al. "Myofibroblasts and mechano-regulation of connective tissue remodelling." *Nature reviews molecular cell biology* 3.5 (2002): 349-363.

Vleeming, A., V. Mooney, and R. Stoeckart, eds. *Movement, stability & lumbopelvic pain: integration of research and therapy*. Edinburgh, Scotland: Churchill Livingstone, 2007.

Vleeming, A., et al. "The posterior layer of the thoracolumbar fascia| its function in load transfer from spine to legs." *Spine* 20.7 (1995): 753-758.

Wang, Y., et al. "Hyperelastic material properties of mouse skin under compression." *PLOS ONE* 8.6 (2013): e67439.

Ward, S. R., et al. "Passive mechanical properties of the lumbar multifidus muscle support its role as a stabilizer." *Journal of biomechanics* 42.10 (2009): 1384-1389.

Westneat, M. W., et al. "Mechanics of the fast-start: muscle function and the role of intramuscular pressure in the escape behavior of amia calva and polypterus palmas." *Journal of experimental biology* 201.22 (1998): 3041-3055.

Willard, F. H., et al. "The thoracolumbar fascia: anatomy, function and clinical considerations." *Journal of anatomy* 221.6 (2012): 507-536.

Yahia, L. H., P. Pigeon, and E. A. DesRosiers. "Viscoelastic properties of the human lumbodorsal fascia." *Journal of biomedical engineering* 15.5 (1993): 425-429.